Summer 2017

Ab Initio Methyl Linoleate Bond Dissociation Energies: First Principles Fishing for Wise Crack Products

Zachary Ryan Wilson
Missouri State University, Wilson333@live.missouristate.edu

AB INITIO METHYL LINOLEATE BOND DISSOCIATION ENERGIES: FIRST PRINCIPLES FISHING FOR WISE CRACK PRODUCTS

A Masters Thesis

Presented to

The Graduate College of

Missouri State University

In Partial Fulfillment

Of the Requirements for the Degree

Master of Science, Chemistry

By

Zachary R. Wilson

August 2017

AB INITIO METHYL LINOLEATE BOND DISSOCIATION ENERGIES: FIRST PRINCIPLES FISHING FOR WISE CRACK PRODUCTS

Department of Chemistry

Missouri State University, August 2017

Master of Science

Zachary R. Wilson

ABSTRACT

With the prices of petroleum reflecting demand for this finite resource, attention has been turned to alternative sources of energy. Biodiesel, defined as fatty acid methyl esters (FAMEs), exhibits many of the same properties as conventional diesel but is derived from biological sources. FAMEs are subsequently thermally cracked to form more light-weight petrochemical products. I aim to further understand the thermal cracking procedure, at an atomic-level, in hopes that this may aid in future engineering of viable fuels. I studied the effective computational modeling of bond disassociations in the FAME methyl linoleate. Bond dissociation in a 44-reaction database with known experimental energies were used to evaluate density functional (B3LYP, M06-2X, B97D), wavefunction (MP2), and composite methods (G3 and CBS-QB3). I found that the M06-2X/ 6-31+G(d,p) model chemistry provides results comparable to the composite CBS-QB3 method at a much reduced cost. Data were then compiled for possible bond dissociations in FAME methyl linoleate. Lastly, atom-centered density propagation (ADMP) trajectory calculations were performed to obtain a statistical evaluation of thermal cracking products of methyl linoleate. As a result, I have parameterized an effective methodology to evaluate the thermal cracking process of FAMEs.

KEYWORDS: biodiesel, thermal cracking, pyrolysis, alternative energy, molecular dynamics, ADMP, M06-2X, methyl linoleate, density functional theory, computational, theoretical

This abstract is approved as to form and content

_____

Matthew R. Siebert, PhD.
Chairperson, Advisory Committee
Missouri State University

AB INITIO METHYL LINOLEATE BOND DISSOCIATION ENERGIES: FIRST PRINCIPLES FISHING FOR WISE CRACK PRODUCTS

By

Zachary R. Wilson

A Masters Thesis
Submitted to the Graduate College
Of Missouri State University
In Partial Fulfillment of the Requirements
For the Degree of Master of Science, Chemistry

August 2017

Approved:

_____
Matthew R. Siebert, PhD, Committee Chairperson

_____
Kevin Evans, PhD, Committee Member

_____
Eric Bosch, PhD, Committee Member

_____
Dean Cuebas, PhD, Committee Member

_____
Julie Masterson, PhD: Dean, Graduate College

ACKNOWLEDGEMENTS

I would like to thank the whole of Dr. Siebert's lab. It is my wish that the level of support that was afforded me can remain a part of the culture of this lab. Without the assistance of Dr. Siebert and my fellow researchers, I would still be struggling to understand even the basic tenants of quantum chemistry.

I wish to also thank my wife, Kelly Rose, who put up with me during the long trek to complete a Master's Degree in Chemistry. How I got so lucky will remain a great mystery of the Universe.

I dedicate this thesis to Jeffrey Mark Wilson. I will never forget my loving and supportive father who nurtured a love of science and a desire to "do the crazy thing" with life. I will always miss you.

TABLE OF CONTENTS

Chapter 1: Foundations 1
- 1.1 Introduction 1
- 1.2 Model Chemistry 4
- 1.3 Problems with Current Methodologies 8
- 1.4 Experimental Precedence 14
- 1.5 Molecular Dynamics 16

Chapter 2: Methodology 28
- 2.1 Evaluated Methods 28
- 2.2 ADMP Parameterization 30

Chapter 3: Results and Discussion 32
- 3.1 Benchmark Studies 32
- 3.2 Bond Dissociation Studies 36
- 3.3 ADMP Trajectory Studies 37

Chapter 4: Summary and Conclusions 46

References 47

Appendices 55
- Appendix A. B3LYP Benchmark Data 55
- Appendix B. M06-2X Benchmark Data 56
- Appendix C. B97-D Benchmark Data 57
- Appendix D. MP2 Benchmark Data 58
- Appendix E. CBS-QB3 Benchmark Data 59

LIST OF TABLES

TABLE 1. Mean Average Percent Deviations (MAPDs) in Calculated Homolytic Bond Dissociation Energies (BDEs) for Chemical Moiety Representative (CMR) Reactions 1 – 44. 34

TABLE 2. Mean Average Percent Deviations (MAPDs) in Calculated Homolytic Bond Dissociation Energies (BDEs) for Chemical Moiety Representative (CMR) Reactions 1 – 44 Separated by Bond Type. 35

LIST OF FIGURES

FIGURE 1. Fats and/or oils undergo transesterification in the presence of methanol and a catalyst to form the commodity chemical glycerol and fatty acid methyl esters (FAMEs; biodiesel). The exact identities of the FAMEs depend on the identity of the fat or oil used. 2

FIGURE 2. The structure of methyl linoleate, the FAME most prevalent in the most common biodiesel stock for the United States. 3

FIGURE 3. Description of Electron Correlation Processes. 9

FIGURE 4. Examples of the Effects of Protobranching on Stability of Molecules. 11

FIGURE 5. Performance of Methods with Protobranching Effects (As Reproduced from Reference 41) 13

FIGURE 6. Observed Products for the Thermal Cracking of Common FAMEs 15

FIGURE 7. Chemical Moiety Representative (CMR) Reactions with Structural Resemblance to Fatty-Acid Methyl Esters (FAMEs) Methyl Linoleate and have Experimental Bond Dissociation Energies (BDEs) Reported 33

FIGURE 8. M06-2X/6-31+G(d,p) optimized structure. BDEs displayed in kcal/mol. 36

FIGURE 9. Atomic naming scheme to describe bond scissions during the thermal cracking of methyl linoleate....37

FIGURE 10. Products formed during parameterization trajectories at 3500 K....38

FIGURE 11. Products formed during parameterization trajectory at 3750 K. 39

FIGURE 12. Products formed during parameterization trajectories at 4000 K....41

FIGURE 13. Products formed during productive production trajectories. 44

CHAPTER 1: FOUNDATIONS

1.1 Introduction

Biodiesel. Crude oil, and the products derived from it, drive much of our modern society. The refining process provides us with, e.g., commodity chemicals precursors for plastics used in everyday life, natural gas used to heat homes and cook food, and the fuel used for transportation. However, the current supply of crude oil is both finite and in high-demand as the population grows and develops.[1-11] The process of extracting crude oil from the Earth is a very costly endeavor as it involves locating, drilling, transporting, and refining.[2, 4] The environmental impact of utilizing crude oil has also proven to be very costly. Among its many impacts fossil-based fuels are extracted from the ground, resulting in previously-sequestered carbon entering the atmosphere to contribute to global warming effects.[5-6, 8-10, 12-18]

All of the above motivates society to find an alternate source of transportation fuel. One of these possible solutions may be biofuels;[1, 3, 5-10, 12-14, 16-23] the biofuel with, perhaps, the most promise is biodiesel. Biodiesels are a mixture of fatty-acid methyl esters (FAMEs) derived from naturally occurring fats and/or oils.[1, 3, 6-10, 12-25] These FAMEs are characterized by containing monoalkyl chains 12-20 carbons in length.[23]

Biodiesel compounds have many favorable qualities as a transportation fuel. First, synthesis of biodiesel is a renewable resource.[8, 10, 12-14, 17, 19] Given that the triglycerides used to produce biodiesel are often formed by photosynthesis,[1, 3, 6, 24] the process of synthesizing biodiesel is a carbon-neutral process.[6, 18] Biodiesel is, reportedly, less

hazardous to the environment than traditional diesel fuel.[5, 7-10, 12-18] Further, the emissions generated by biodiesel contain less SO_X compounds and soot particles.[5, 8-10, 12-15, 17-18]

Synthesis of FAMEs occurs via transesterification of a triglyceride with methanol and a catalyst[1, 3, 5-10, 12-21, 23-24] liberating glycerol (a commodity chemical itself).[3] Although either an acid or a base can be used to catalyze transesterifaction, industrially catalysis is affected by bubbling hydrochloric acid followed by sodium hydroxide.[7, 18] The identity of the FAMEs produce by transesterification is dependent upon the triglyceride.[12, 15, 18]

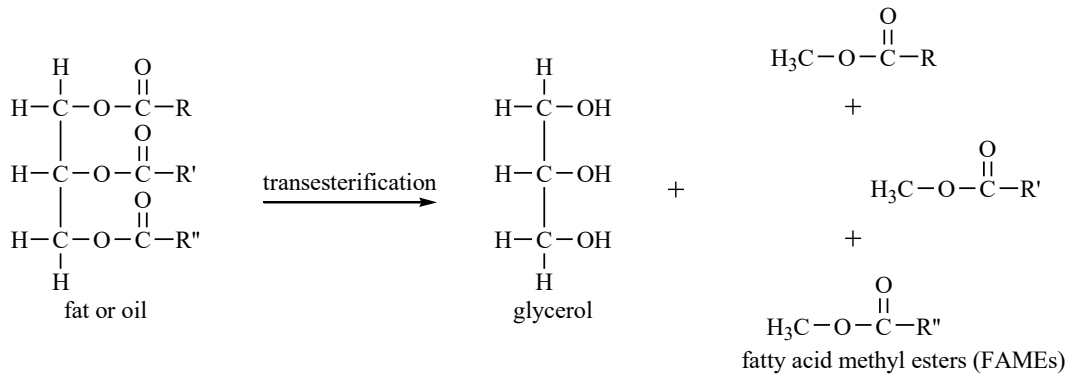

FIGURE 1. Fats and/or oils undergo transesterification in the presence of methanol and a catalyst to form the commodity chemical glycerol and fatty acid methyl esters (FAMEs; biodiesel). The exact identities of the FAMEs depends on the identity of the fat or oil used.

In the United States, the most common source of triglyceride stock is soybean oil.[3, 10, 16, 20-21] Linoleic acid appears in the largest proportion in soybean oil at 52 – 56% w/w (23.0 – 25.0% w/w oleic acid).[15, 19] In Europe, the main biodiesel feedstock is canola oil and its largest constituent is oleic acid (60.0 – 64.3% w/w), which is comprised of 19.1 – 20.0% w/w linoleic acid.[3, 10, 16, 20-21] As linoleic acid appears in the largest proportion in the most commonly used stock in the United States and second largest in Europe, this study will focus on the methyl ester of linoleic acid (Figure 2).

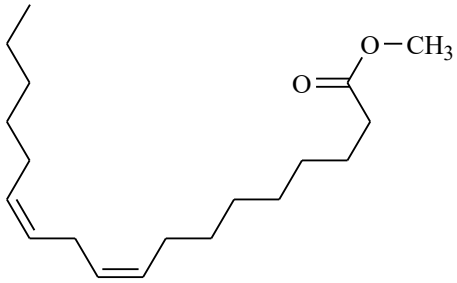

methyl linoleate

FIGURE 2. The structure of methyl linoleate, the FAME most prevalent in the most common biodiesel stock for the United States.

For all of the positive attributes of biodiesel listed above, there are several negative attributes. For example, biodiesel combustion is observed to produce higher proportions of NO_X compared to fossil fuel.[5, 9, 12-18] Additionally, the typical pour point (the point where fuel becomes a gel) is -9 to 15 °C, which hinders its use in cold climates.[1, 12, 15, 26] The amphiphilic nature of biodiesel leads to its action as a surfactant that can dislodge engine deposits resulting in possible damage. Retrofitting of engines to avoid this can be cost prohibitive, which may be one of the hindrances to biodiesel availability in our current infrastructure.[3, 9, 13] Many of these detriments to the use of biodiesel might be alleviated by thermal cracking of the FAMEs to lower molecular-weight products, including transportation fuels, plastic precursors, natural gas, kerosene, and possibly gasoline.[5-6, 9, 14, 16-17, 19-20]

Thermal Cracking. Thermal cracking, also known as pyrolysis, [5, 11, 22, 25, 27-29] uses thermal energy to break down larger molecules into smaller hydrocarbons.[16-17, 19-22, 29-32] This process is already utilized in the petroleum refining industry. It is dominated by radical mechanisms as thermal energy propagates through the molecular system causing homolytic bond cleavages.[14, 16, 20-22, 25, 29, 31-33] This will produce a wide array of low- to

medium-weight hydrocarbon products that resemble those derived from processing of fossil oil, some of which resemble the constituents of gasoline (hydrocarbons containing 4 – 12 carbons).[3]

1.2 Model Chemistry

Total Energy Operators. The wave-particle duality behavior of electrons cannot be ignored when discussing molecular orbitals. To address this behavior, the molecular electronic structure is seen not as a bunch of moving particles, but as a wave. To this end, the quantum mechanical systems of a molecule could be treated similar to wave mechanics as outlined by Newtonian physics. All information about the state of the molecular system could be derived from a single term called the wavefunction (Ψ). To extract information about the state described by the wavefunction, a quantum mechanical operator is used to operate on the wavefunction. After this operation is complete, the original wavefunction (the eigenfunction) remains with an extra term that is fully separable from the original wavefunction (the eigenvalue). The eigenvalue derived from the operation is the measurable property designated to the quantum mechanical operator. [43, 45]

One of the most noted examples of this is the time-independent Schrödinger equation. Both the general form and the expanded form are presented in eq 1 and 2. In the general equation, $\hat{H}$ is the Hamiltonian (total energy) operator, and E is the total energy eigenvalue of the system. In the expanded equation: $\hbar$ Planck's constant divided by 2π, m_e is the mass of an electron, ∇ is the Laplacian operator$\left(\frac{\partial^2}{\partial x^2} + \frac{\partial^2}{\partial y^2} + \frac{\partial^2}{\partial z^2} \right)$, r is a position vector, and V is the potential energy term. [43, 45]

$$\hat{\mathrm{H}}\Psi = \mathrm{E}\Psi \tag{1}$$

$$\left(-\frac{\hbar^2}{2m_e}\nabla^2 + V_{(r)}\right)\Psi_{(r)} = E\Psi_{(r)} \tag{2}$$

However, a more complex version of the Hamiltonian operator is generally employed to evaluate the total energy of a molecular system more thoroughly. In eq 3: i and j refer to the electrons, k and l refer to the nuclei in the molecule, Z refers to the atomic number, r refers to the radius between particles, and e refers to the charge of an electron. The first term discusses the kinetic energy of electrons, the second term discusses the kinetic energy of the nuclei, the third term discusses the columbic attraction between electrons and the nuclei, the fourth term discusses the repulsion and correlation of electrons to one another, and the final term discusses the internuclear repulsions of nuclei. [43, 45]

$$H = -\sum_i \frac{\hbar^2}{2m_e} - \sum_k \frac{\hbar^2}{2m_k} - \sum_i \sum_k \frac{e^2 Z_k}{r_{ik}} + \sum_{i<j} \frac{e^2}{r_{ij}} + \sum_{k<l} \frac{e^2 Z_k Z_l}{r_{kl}} \tag{3}$$

Due to the significant mass difference between electrons and nuclei, the Born-Oppenheimer (BO) approximation can be invoked to keep the radii between nuclei constant rather than dynamic. It also renders the kinetic energy of the nuclei to have a value of zero while simultaneously eliminating electron-nucleus correlation. This simplifies the Hamiltonian operator by eliminating all but the first, third (which becomes a constant) and fourth terms. With the BO approximation in effect, the Schrödinger

equation can be expressed purely in terms of electronic energy in the form of the electronic Schrödinger equation (as mentioned in eq 4). The subscript "el" denotes that the BO approximation is in effect. The term V_N represents the nuclear-nuclear repulsion as a constant. The terms $\mathbf{q_i}$ and $\mathbf{q_k}$ are electronic coordinates as independent variables and nuclear coordinate parameters, respectively. The E_{el} term is known as the "pure electronic energy". If the V_N term is combined with the E_{el} term, it is known as simply the "electronic energy". [43, 45]

$$(H_{el}V_N)\psi_{el}(\boldsymbol{q}_i{:}\,\boldsymbol{q}_k) = E_{el}\psi_{el}(\boldsymbol{q}_i{:}\,\boldsymbol{q}_k) \quad (4)$$

The issue that arises from the Schrödinger equation is that the mathematical treatment of every electron in a molecular system is impossible (with the noted exception of hydrogen). The repulsion between every electron, known as electron correlation, is currently unsolvable for many-body systems. The Hartree-Fock (HF) method ignores electron correlation by treating every electron as a single electron orbital. This allows HF to focus on electron exchange, which are the collection of electronic interactions other than electron correlation. Density functional theory (DFT), many-body perturbation theory (MBPT), and hybrid DFT rely on different methods that can describe parts of electron correlation and exchange, but not both completely. Different methods can excel in the description of certain systems while fail at describing others. Therefore, methods should be evaluated for their description of similar systems before use. [43, 45]

Basis Sets. Collectively, the number and type of atomic orbitals used to construct the molecular orbitals from the linear combination of atomic orbitals (LCAO) is what

constitutes a “basis set”. The molecular orbitals expressly equal the wavefunction, which describes the electronic system. The combination of a total energy operator and a basis set is known as a “model chemistry”. Together, they represent an approximated total energy operator operating on the wavefunction (as generated by the atomic orbitals of the basis set). To describe these atomic orbitals mathematically, Slater-type orbitals (STOs) are approximated by the combination of atom-centered Gaussian functions. This allows for the accurate portrayal of electronic densities as the nucleus is approached. Typically, the larger the number of summed Gaussian functions, the more accurate the portrayal of the molecular orbital structure. [43, 45]

The generated wavefunction does not have to incorporate atom-centered Gaussian functions. Plane-wave basis sets are created by generating the wavefunction as a periodic wave stationed over the molecular system. This is permitted by the invocation of the quantum mechanical “particle-in-the-box” approximation. However, this study will only involve atom-centered STOs. [43, 45]

1.3 Problems with Current Methodologies

B3LYP. Quantum chemical methods have been used to calculate bond dissociation energies (BDEs) to describe the thermochemical properties of FAMEs. Currently, most of these methods use B3LYP.[16-17, 20, 22, 25, 29, 32, 34-37] There has been recent literature using the B3LYP/6-31G(d,p),[16, 20] B3LYP/6-311G(d,p),[32, 34-35, 37] and B3LYP/6-311G+(2d,p)[22] methods to describe bond dissociations in methyl linoleate and similar systems. Considering the limitations of B3LYP, we wish to evaluate other methods to determine their viability in describing the thermochemical properties of methyl linoleate.

The limitations of the B3LYP functional involve its deficiencies in describing π-bonded conjugated systems, Van der Waals forces, large systems,[43-45] and 1,3-dialkyl interactions known as "protobranching".[38-42]

Protobranching. One of the processes we want to investigate as a possible source of error for our calculations of thermochemical properties is "protobranching". The definition of protobranching is the sum of all the 1,3-alkyl-alkyl group interactions present in a molecule. [38-42] This definition excludes methane and ethane because they lack 1,3-alkyl-alkyl group interactions. [38-43] This report will discuss the cause of protobranching, the problems posed to calculating thermochemical properties by protobranching, and possible solutions to address the problem of protobranching.

One of the effects protobranching has on alkanes is that the process tends to provide more stability to branched alkanes rather than linear alkanes. [38-43] As mentioned before, protobranching is the sum of all 1,3-alkyl-alkyl group interactions in a molecule. These 1,3-alkyl-alkyl group interactions come from bond interactions with neighboring atoms (within 1.5 to 3.0 Å) and their molecular bonds. [42] It has been observed that there is evidence of intrapair electron correlation between C-C bonds. Also, similar interactions have been observed with vicinal and 1,3-alkyl-alkyl group interactions between C-H and C-H bonds. These electron correlation processes have been theorized to occur through their localized molecular orbitals (LMOs). Geminal correlation, as described in Figure 3, between 1,2 C-C and C-H molecular bonds have been found to have a near zero contribution towards the overall effect of protobranching. [42] This surprising level of hyperconjugation tends to lead to a more stable molecule at these branching points. This begins to present a problem to computational chemists because many thermochemical

calculation methods either do not take electron correlation into account (or the process is simply approximated), which leads to systematic error. Even in linear alkanes, the stability can rise from the protobranching effect by roughly 2.8 kcal/mol for every homologation (addition of another $–CH_2-$ unit to the chain). [38-41] The driving force behind protobranching (and the extra stability it provides) is a result of electron correlation, which is a possible major cause of error in calculating thermochemical properties. [38-43]

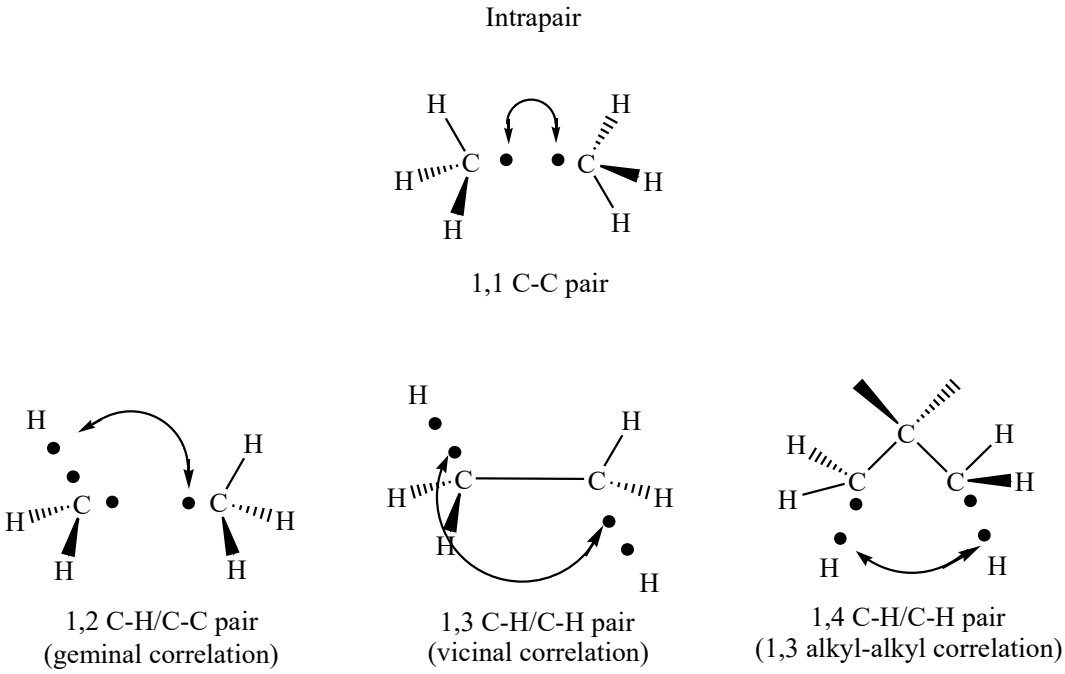

FIGURE 3. Description of Electron Correlation Processes

Protobranching also has an appreciable effect in when performing calculations of thermochemical properties on ring structures. [42] Cyclohexane is generally regarded as an example of a "zero strain" cycloalkane because of the tetrahedral geometry of its constituents. [42] However, Figure 4 demonstrates that there is evidence against this argument. Instead of demonstrating zero ring strain between the bonds in cyclohexane,

the process of 1,3 alkyl-alkyl group interaction *via* electron correlation presents a stabilizing effect to the ring structure. This provides a "negative strain" on the ring structure, providing a more stable molecule than previously thought. In Figure 3, the isodesmic reaction of 6 ethane molecules being compared to 6 methane and one cyclohexane molecule yields an energy difference of -18.17 kcal/mol in favor of the formation of cyclohexane. [42] Similar strong stabilization effects can be observed when comparing ethane to propane, butane to isopropane, and pentane to neopentane. This demonstrates the powerful effect protobranching can have when considering the stabilizing effect of electron correlation processes. [38-40, 42, 43] During the process of thermal cracking, some of the predicted reaction byproducts are cycloalkanes and branched alkanes. [44] With a better understanding of the quantum behavior of cycloalkanes and other protobranching alkanes, a more informed decision on what method would be appropriate to perform our thermochemical calculations.

The phenomenon of protobranching can cause theoretical calculations, such as bond dissociation energy (BDE), to contain great errors in accuracy. [38-43] Errors in calculating thermochemical properties can happen because HF and most DFT calculations underestimate the stabilizing effect of branched alkanes. [38, 41, 43] This is because HF does not take into account the effect of electron correlation at all in favor of focusing on electron exchange calculations. DFT methods have a tendency to only provide an approximation of the effects of electron correlation rather than explicitly including electron correlation calculations. [38, 41, 43] In order to get better results in

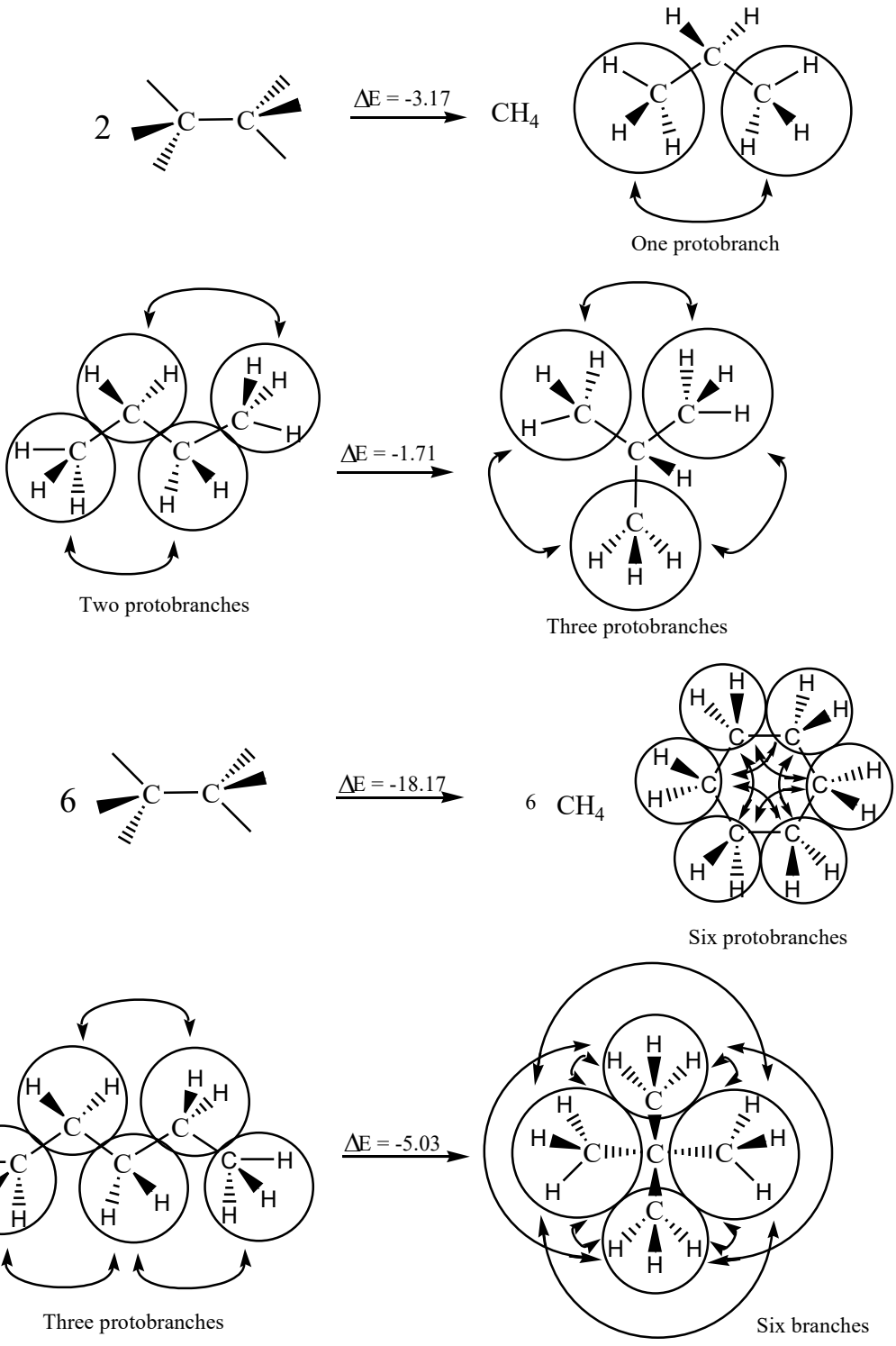

FIGURE 4. Examples of the Effects of Protobranching on Stability of Molecules [40, 42]

calculating thermochemical properties, a level of theory must be selected that contains accommodations for electron correlation without being overly computationally expensive.

The greatest success with BDE calculations where protobranching is known to have a large effect has been with *ab initio* post Hartree-Fock methods (WFT) that explicitly include electron correlation in their calculations *via* empirical corrections. This treatment can approximate the effects of protobranching very effectively. These methods include, but are not limited to: MP2, SCS-MP2, Expt, SVWN5, G3 and CCSD (coupled cluster method family). [38-43] Methods that do not adequately describe electron correlation, as described in Figure 5, systematically perform with lower accuracy as the number of protobranching groups is increased. [41] The methods that do account for electron correlation seem to maintain accuracy with each added protobranching group. [41] Some of the calculations mentioned to be effective in accounting for the effects of protobranching have been demonstrated to be computationally expensive. However, these methods have been demonstrated to be largely effective in accounting for the effect of protobranching in BDE calculations. [38, 41]

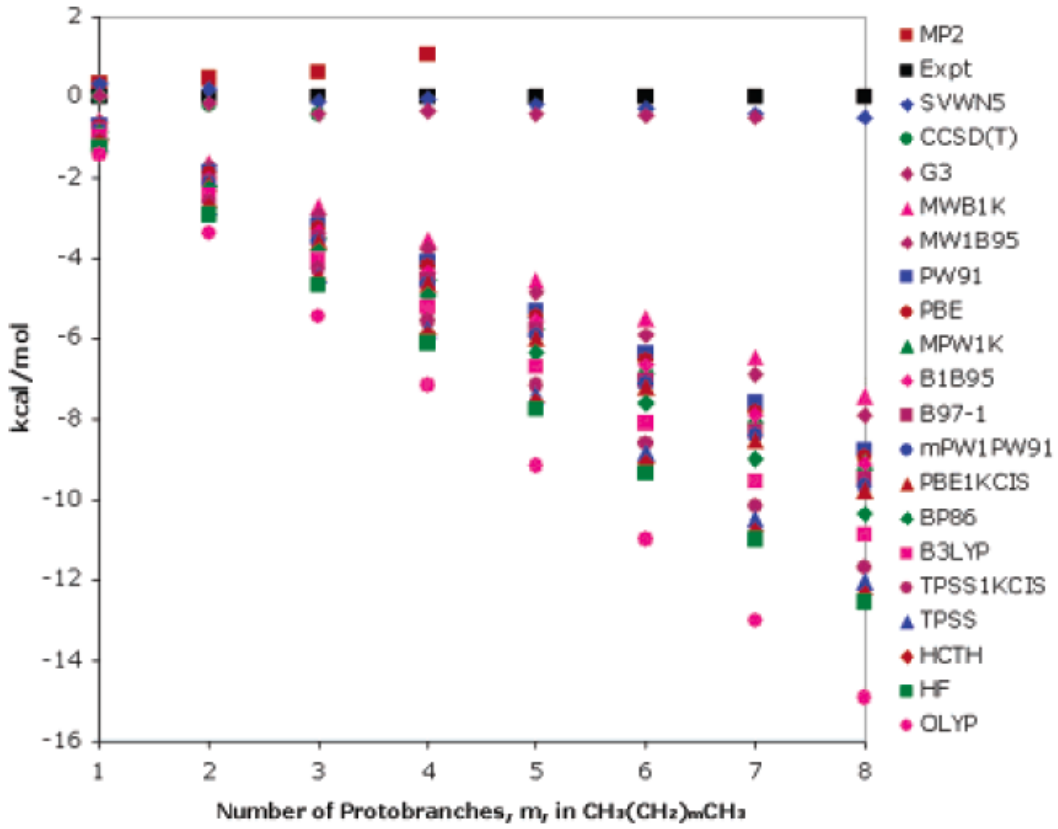

FIGURE 5. Performance of Methods with Protobranching Effects (As Reproduced from Reference 41)

ReaxFF Methodology. Another method that has been proposed is known as the ReaxFF method. This method relies on the relationship between bond distance and bond order to predict homolytic bond scissions for hydrocarbon systems.[22, 25, 32-33, 37] Other variables such as bond angles and dihedral angles are also parameterized to the predicted bond orders of the system.[33] This information is then used to perform molecular dynamic (MD) trajectory calculations to predict bond cleavages.[22, 32, 34-35, 37] However, the method that was used to parameterize these values was B3LYP/6-311G**.[32, 37] The ReaxFF method would be inappropriate to describe the thermal cracking of methyl linoleate due to the limitations of the B3LYP method.

1.4 Experimental Precedence

Observed Products. The theoretical aspects of the thermal cracking process has been confirmed for the pyrolysis of soybean and canola seed-derived triglycerides. During this procedure, the triglycerides were thermally cracked at 430-440° C to produce a range of hydrocarbon products. The procedure produced 4-7 wt % of gas-phase products. 15-20 wt % was produced as a tar-like solid product. The polar phase formed approximately 5 wt % of the mixture. The remaining 68-76 wt % of the pyrolysis products were organic liquid products (OLP). GC analysis was performed on the OLP layer to determine the products formed during the thermal cracking process. Of these OLPs, approximately 20 mol % are alicyclic, aromatic, or polycyclic aromatic hydrocarbons (PAH). In the OLP layer, are compounds associated with low to middle-weight transportation fuels. Along with these transportation compounds, there are commodity chemicals present that can be used as plastic precursors and other organic reagents. Chart 1 demonstrates the variety of compounds in the OLP layer. [80]

Application to Project. This study aims to determine an accurate yet cost-effective *ab initio* method to describe the thermochemical properties that govern the thermal cracking process for the most prevalent FAMEs in the most common biodiesel stock for the United States. Computational cost is of the utmost importance here as in subsequent studies the attention will be turned to chemical dynamics simulations. This will lead to further understanding of the thermal cracking procedure on an atomic level, which may aid in future engineering of viable fuels.

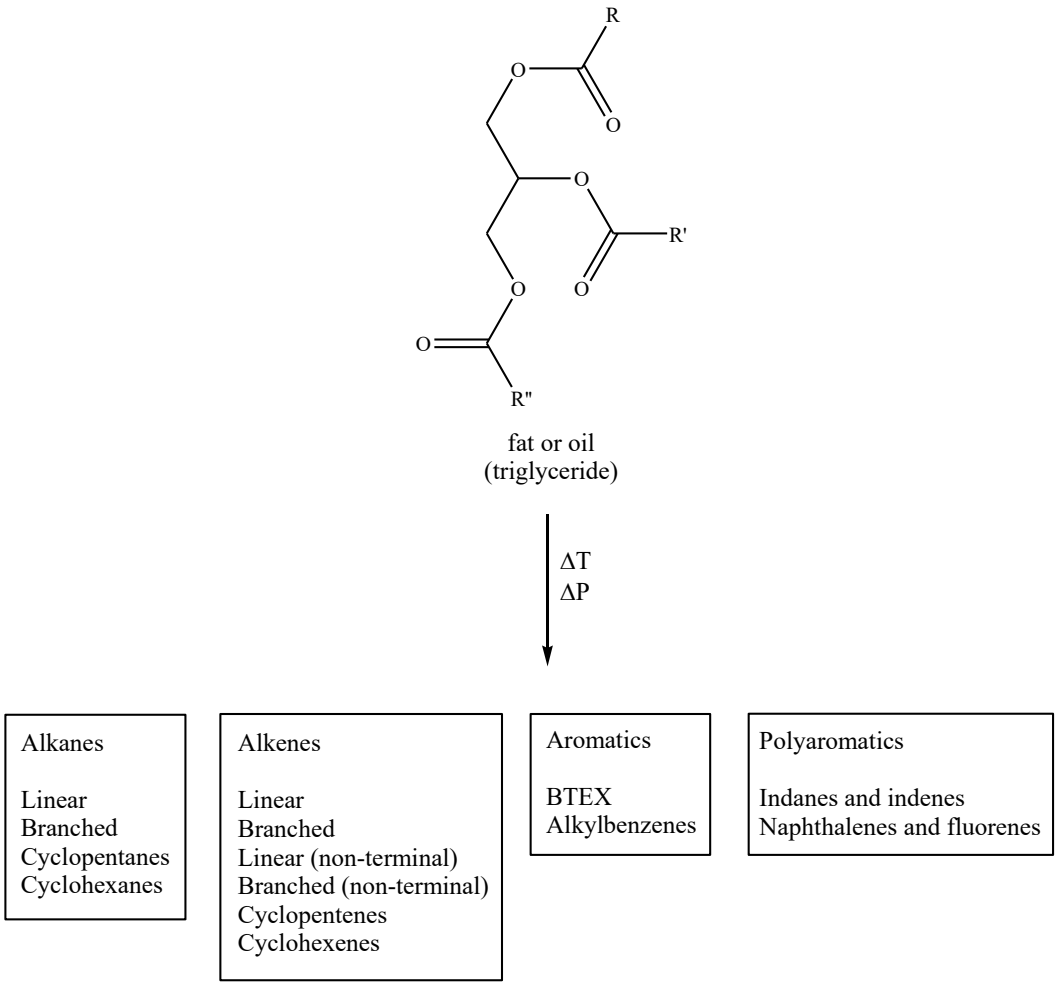

FIGURE 6. Observed Products for the Thermal Cracking of Common FAMEs

1.5 Molecular Dynamics

Classical Molecular Mechanics. To further understand the thermal cracking process, MD simulations were employed. A chief advantage of modeling the thermal cracking process with MD simulations are that you observe the structural changes as they evolve with time. A single MD run, or trajectory calculation, does not provide enough information to describe the thermal cracking process accurately. Instead, an ensemble of trajectories must be completed. Our goal is to parameterize an MD methodology that best describes the thermal cracking process. Then, our next goal is to complete 100 trajectory

calculations of the thermal cracking of methyl linoleate. This should provide a statistically relevant distribution of most likely products of the thermal cracking process. Typical MD simulations use Newton's Laws of Motion to describe the energetics of molecular systems.[54,55] However, due to their highly parameterized nature and lack of quantum mechanical treatment of their atoms, classical MD are not suitable to describe bond breakage and formation.[54,55,64] To model these quantum-chemical behaviors, *ab initio* molecular dynamic (AIMD) simulations are required. A discussion of classic MD is necessary to adequately describe AIMD methodologies.

Classical molecular mechanics rely on Newton's laws of motion and previously parameterized values to describe the thermodynamic and structural properties of their molecular systems.[54] The energy of a system, as described by the MD simulation, is in terms of potential energy.[55] This potential energy, U_{Tot}, is typically partitioned into 5 different potential energies according to eq 5. These partitioned potential energies are the sum of the potential energies present in the bonds (U_r), the bond angles (U_θ), the torsion angles (U_T), the long-range repulsion and attractive interactions (U_{LJ}), and the columbic interactions between atoms (U_E). [55]

$$U_{Tot} = U_r + U_\theta + U_T + U_{LJ} + U_E \tag{5}$$

U_r represents the sum of the potential energies present in the bonds between atoms. This term is an extended version of Hooke's Law as applied to MD. Eq 6 describes the methodology for determining U_r. The term k_{ij}^r is analogous to the Hooke's Law constant, which is a parameterized value for the "compressibility" of the bond. Each

type of bond will have its own unique parameterized value, based on experimental procedure. The term r_{ij} refers to the instantaneous bond distance between atoms *i* and *j*. The term r_{eq} refers to the parameterized equilibrium bond distance for the given bond. [54, 55] This treatment is applied to each bond in the system, where the individual energies are summed to form U_r. [54, 55]

$$U_r = \frac{1}{2}\sum_{Bonds} k_{ij}^{r}\left(r_{ij} - r_{eq}\right)^2 \tag{6}$$

The next term in the U_{Tot} equation defines the sum of the potential energies stored in the bond angles of the system, U_θ. Again, U_θ is based on Hooke's Law. The term k_{ijk}^{θ} represents the Hooke's Law constant for the bond angle formed between atoms *i*, *j*, and *k*. θ_{ijk} refers to the instantaneous bond angle, where θ_{eq} refers to the parameterized bond angle.[54, 55]

$$U_\theta = \frac{1}{2}\sum_{Bonds} k_{ijk}^{\theta}\left(\theta_{ijk} - \theta_{eq}\right)^2 \tag{7}$$

The following term, U_T, refers to the sum of the potential energies present in the torsion angles of the system. This term corrects for steric interference that prevents absolute free rotation of the bond structure of the system. For some molecular dynamics methodologies, this term is divided into two different terms in the form of a proper and an improper dihedral potential energy term.[54] However, for simplicity of the discussion, attention will be given to the more general term as presented in eq 8.[55]

$$U_T = \frac{1}{2} \sum_{Torsion\ Angles} \sum_{m} k_{ijkl}^{\phi,m} \left(1 + cos\left(m\phi_{ijkl} - \gamma_m\right)\right) \quad (8)$$

The U_T term has similarities to the Hooke's Law equation, but it allows for the periodic nature of steric repulsion to be expressed during bond rotation. Much like before, the $k_{ijkl}^{\phi,m}$ term represents the Hooke's Law constant that has been parameterized for a certain bond dihedral angle for atoms *i*, *j*, *k*, and *l*. The m parameter controls the periodicity of resistance during rotation of the dihedral, which correlates to the constituents on the neighboring atoms. ϕ_{ijkl} represents the dihedral's degree of rotation. The γ_m term is a parameterized value that fits the periodic function to the full dihedral degrees of rotation as a "phase shift" term.[55]

The next term describes the long-range repulsion and attractive interaction of neutral non-bonded atoms (intramolecular effects) or other molecules (intermolecular effects). This potential energy term is known as the Lennard-Jones potential, and is denoted as U_{LJ} in eq 5. The equation describing U_{LJ} is outlined in more detail in eq 9. The ε term is a parameterized value for the potential energy well depth between the interacting atoms. σ represents the distance at which the potential between the two atoms are parameterized to zero. The r value represents the instantaneous distance between the two interacting atoms.[54, 55]

$$U_{LJ} = 4\varepsilon \left[\left(\frac{\sigma}{r}\right)^6 - \left(\frac{\sigma}{r}\right)^{12}\right] \quad (9)$$

The final term, U_E, describes the coulombic interactions between atoms. By describing the electrostatic interactions present between the atoms, quantum effects such as hydrogen bonding and other polar interactions can be described through molecular mechanics. The electrostatic interactions between atoms are typically described with eq 10. Q_1 and Q_2 are the electronic charges of the interacting atoms, which allows for the description of either attraction or repulsion based on charge. The term ϵ_0 is the permittivity of space and r is the distance between the two interacting atoms.[54, 55]

$$U_E = \frac{Q_1 Q_2}{4\pi\epsilon_0 r} \tag{10}$$

To describe the forces acting on the individual atoms in a system, a negative partial derivative of U_{Tot} with respect to the coordinates of the atoms is calculated. This acts as an application of the classical Newton's equation of motion to use energy to describe the forces acting on the atoms. This equation is displayed in eq 11.[55]

$$f_i = -\frac{\partial U_{Tot}}{\partial r_i} \tag{11}$$

To calculate positions, velocities, and accelerations at any given time during the molecular dynamic simulation, a thorough but efficient numerical integration algorithm is necessary. A widely used numerical integration algorithm that is used for this purpose is the velocity Verlet integrator. This algorithm is often preferred to other algorithms due to its efficiency in calculation without sacrificing precision. This algorithm has seen

extended use in both classical and AIMD simulations due to the computational cost of the inclusion of quantum mechanical descriptions to the molecular dynamic calculations.[55, 64]

***Ab Initio* Molecular Dynamics.** Classical molecular mechanics and AIMD have different appropriate areas of application. Classical mechanics is appropriate for use in describing large systems (hundreds or even thousands of atoms).[54] AIMD calculations are only appropriate for small molecular systems. This is because of the rigorous quantum mechanical treatment of the molecular systems (less than 100 atoms). This treatment causes AIMD calculations to command a far larger computational cost than classical MD.[54, 57-59] Both classical MD and AIMD are capable of accurately describing geometric conformations of molecular systems. However, the true strengths of AIMD simulations are found in the quantum mechanical descriptions of the electronic wavefunction. This allows for very accurate physical descriptions of systems that are calculated from "first principles", rather than relying on previously parameterized values.[56, 59] This is completed by computing the forces acting on the individual atoms in a system *via* electronic structure calculations. These electronic structure calculations are performed "on-the-fly" during each step of the MD trajectory.[57-59] This also allows for the accurate description of chemical phenomena such as bond breakage and bond formation.[56-59] Classical molecular mechanics, without specific parameterized values, is incapable of describing the quantum mechanical effects necessary for a bond breakage or formation to occur.[54]

The quantum mechanical treatment of AIMD requires the generation of forces on each atom in the system.[58] A quantum mechanical analog to the classical Newton's equation of motion is provided in eq 12. In this equation, the force is calculated by multiplying the mass of the atom (M_I) with the instantaneous velocity of the atom (R'_I).

In *lieu* of a U_{Tot} potential energy term, there is a $U(R, \rho^{SC})$ term known as the BO potential energy. This term represents the potential energy as calculated from quantum-chemical methodologies as a function of the instantaneous atomic geometry and the relaxed self-consistent ground state electronic density. This BO potential energy is then operated on with a negative partial derivative with respect to the instantaneous atomic coordinates to produce the 3 different forces exerted on the atoms during AIMD.[57-58]

$$M_I \mathrm{R'}_I = -\frac{\partial U(R, \rho^{SC})}{\partial R_I} \tag{12}$$

To calculate intramolecular forces in AIMD, the Hellmann-Feynman equation is used to calculate the Hellmann-Feynman force.[58] The Hellmann-Feynman equation is also responsible for the calculation of the equilibrium geometries and the propagation of the electron density matrix across the molecular system. This is accomplished by including dynamic fictitious variables to the electronic degrees of freedom to allow for a dynamic description of the electronic density at each step of the AIMD trajectory. Once the time-dependent Schrödinger equation is solved, the forces present in the system can be calculated using classical electrostatics. The Hellmann-Feynman equation is outlined in eq 13. λ is defined as the continuous parameter of the equation in the form of the nuclear coordinates. The term E_λ is the eigenvalue of the Kohn-Sham wavefunction of the system. ψ_λ is the eigenfunction of the Kohn-Sham wavefunction, which is implicitly dependent on λ. The term dV implies the integration of the whole Kohn-Sham wavefunction.[58, 61, 62]

$$\frac{dE_\lambda}{d\lambda} = \int \psi_\lambda^* \frac{d\hat{\mathrm{H}}_\lambda}{d\lambda} \psi_\lambda dV \tag{13}$$

Another important equation is the Pulay equation, which describes the Pulay force.[58] This force is only present when the basis set used incorporates atom-centered basis functions, such as Gaussian functions. If plane-wave basis functions are used during the AIMD calculation, this term is null and not present.[58, 60, 78] Eq 14 is the Pulay equation, which allows for the centering of the atom-centered basis functions over the correct nuclear coordinates. The first term is equivalent to the Hellmann-Feynman force, where the second and third terms are known as the "wavefunction force".[78] The Pulay equation is set to the partial derivative of the eigenvalue of the Kohn-Sham wavefunction with respect to the nuclear coordinates. ψ is defined as the Kohn-Sham wavefunction, while R represents the nuclear coordinates. Without this term, the atom-centered basis functions could not describe the electron orbitals present on or between the nuclei.[60, 78]

$$\frac{\partial E}{\partial R} = \left\langle \psi \middle| \frac{\partial H}{\partial R} \middle| \psi \right\rangle + \left\langle \frac{\partial \psi}{\partial R} \middle| H \middle| \psi \right\rangle + \left\langle \psi \middle| H \middle| \frac{\partial \psi}{\partial R} \right\rangle \tag{14}$$

The final force is known as the Residual Term ($\overrightarrow{F_{RT}}$). This term is present during nonadiabatic conditions. This force is null if full self-consistency is reached in the form of a relaxed ground state electronic configuration. If the system is not currently in the relaxed electronic ground state, this Residual Term takes effect to generate corrected forces on each nucleus ($\overrightarrow{F_\alpha}$). The residual term allows for the optimization of the geometry and the return of the system to the relaxed electronic ground state. For this to

occur, corrections accounting for the incomplete basis set ($\overrightarrow{F_\alpha^{IBS}}$) and non-self-consistent charge densities ($\overrightarrow{F_\alpha^{NSC}}$) are needed. $\overrightarrow{F_\alpha^{IBS}}$ nullifies the first-order basis set error initially presented from the calculation of forces on the nuclei. However, this term is null if a plane wave basis set is used. $\overrightarrow{F_\alpha^{NSC}}$ corrects for imperfections in the self-consistency cycle that create distance from the BO surface. These corrections are then directly applied to the forces generated for the individual nuclei ($\overrightarrow{F_\alpha^{HF}}$). The equation describing this process is outlined in eq 15.[78] This term is important for the first class of AIMD, which is known as Born-Oppenheimer molecular dynamics (BOMD).[58, 78]

$$\overrightarrow{F_\alpha} = \overrightarrow{F_\alpha^{HF}} + \overrightarrow{F_{RT}} = \overrightarrow{F_\alpha^{HF}} + \overrightarrow{F_\alpha^{IBS}} + \overrightarrow{F_\alpha^{NSC}} = 0 \qquad (15)$$

BOMD is an AIMD method that requires energy minimization at each step of the calculation to ensure adherence to the BO potential energy surface.[58] This surface is found when the nuclear dynamics are the same as described by the time-dependent Schrödinger equation for the time-dependent nuclear wavefunction.[57] For this condition to be met, the fundamental assumption is that excited electronic states are forbidden along the BO surface.[73]

BOMD has certain advantages and disadvantages. With the inclusion of Pulay forces, atom-centered basis functions are suitable for use for the basis set.[57, 60] However, if tight convergence criteria are not met in regards to the SCF cycle, then the Residual Force can lead to poor energy conservation for the system.[58] The full energy minimization requirement for each time step can greatly increase the computational cost

of the trajectory calculation.[57-58, 67] The second class of AIMD, which is known as extended-Lagrangian molecular dynamics (ELMD), does not have this issue.[57, 73]

ELMD is defined by using extended Lagrangian mechanics to propagate the wavefunction across the classical degrees of freedom of the nuclei.[67, 69, 73] The advantage of ELMD over BOMD is that it is no longer required to complete electronic convergence between each time step. This can increase the efficiency anywhere from 2 to 4 times that of BOMD.[73] However, a full SCF cycle can still be requested to ensure adiabaticity of the system. One of the most common of the ELMD methods is known as Car-Parrinello molecular dynamics (CPMD).

CPMD typically uses plane wave basis sets to describe the dynamic electronic densities. The advantages of using plane wave basis sets are that they nullify the Pulay Forces and make the Residual Forces terms easier to calculate by nullifying the incomplete basis set force correction term. This makes CPMD ideal for describing bulk/extended systems.[57, 78] The disadvantage of using plane wave basis sets is that they do not describe the electronic density accurately close to the nuclei. As the nuclei are approached, plane wave basis sets cannot describe the cusp-like electronic density as accurately as Gaussian functions.[57, 63, 64] Gaussian functions can be used as an adjunct to correct for this effect, but the addition of Gaussian functions can make the trajectory calculations more computationally expensive.[63] Also, the addition of Gaussian functions can lead to poor energy conservation when compared to purely plane wave basis sets. [65] To remove this problem, a new ELMD methodology was developed called atom-centered density matrix propagation molecular dynamics (ADMP).

Eq 16 describes the extended-Lagrangian function that allows for the propagation of the electronic density matrix across the nuclei treated with classical degrees of freedom. Tr denotes a trajectory-dependent term, as the distribution of forces are randomized for each "seed" with a random number generator. $\boldsymbol{V^T MV}$ denotes a momentum-scaling term. μ represents the fictitious mass tensor of the electronic system while $\boldsymbol{W}$ represents the density matrix velocity, leading to a fictitious density matrix momentum for the electronic structure. $E(\boldsymbol{R}, \boldsymbol{P})$ denotes the potential energy as a function of position of the nuclei ($\boldsymbol{R}$) and the single-electron density matrix ($\boldsymbol{P}$), as derived from the selected total energy operator. You are still reading this? I applaud your fortitude. The Lagrangian multiplier matrix (Λ) enforces N-representability, which ensures that electrons are not double-counted. The first two collective terms are known as the kinetic energy terms, while the last two terms are the potential energy terms.[63, 72, 74]

$$L_{ADMP} = \frac{1}{2} Tr(\boldsymbol{V^T MV}) + \frac{1}{2} Tr([\mu^{\frac{1}{4}} \boldsymbol{W} \mu^{\frac{1}{4}}]^2) - E(\boldsymbol{R}, \boldsymbol{P}) - Tr[\Lambda(\boldsymbol{PP} - \boldsymbol{P})] \qquad (16)$$

ADMP has many advantages over the previously described methodologies. As mentioned previously, ADMP uses atom-centered Gaussian basis functions.[64-65, 68] As a further advantage, ADMP was specifically designed for use with Gaussian basis functions as to prevent poor energy conservation during trajectory calculations.[64-65] ADMP also provides the flexibility of either treating each electron in the system separately or using pseudopotentials to describe core electrons.[63] Unlike CPMD, there is no need for use of pseudopotentials on hydrogen atoms or the use of deuterium instead of hydrogen.[63-65, 74] To ensure adherence to the BO potential energy surface, fictitious

masses for the electronic degrees of freedom are set automatically to maintain the electronic ground state throughout the calculation. Good computational efficiency is achieved by using fewer basis functions per atom while implementing larger time steps than CPMD. Despite the increased computational efficiency, ADMP is as accurate as BOMD while maintain similar efficiency as CPMD.[56, 71] ADMP also allows for rigorous on-the-fly control of the deviation from the Born–Oppenheimer surface and the mixing of the fictitious kinetic energies of the electrons and real kinetic energies of the nuclei.[63] The treatment of gas-phase and cluster systems is excellent for ADMP due to the use of Gaussian functions.[63, 71] This is because of the problems that plane wave basis sets, like the ones used in CPMD, have in describing non-periodic molecular systems. Further flexibility is allowed in ADMP because either semi-empirical, HF, pure DFT, or hybrid DFT operators can be used to describe the system of study.[64-65] These advantages can be used to accurately model the thermal cracking of methyl linoleate.

The advantage of modeling the thermal cracking process with ADMP is that it allows for the viewing of geometric and dynamic bond activity as time progresses in the trajectory calculation.[66, 70] Unfortunately, the thermal cracking process occurs experimentally within a 2-6 hour timeframe.[56] The time frame that ADMP can reasonably calculate is in the tens of picoseconds range. However, precedence has been set in the field of computational biology to provide a solution to this problem. This solution is known as temperature-accelerated molecular dynamics method (TAMD).[76-77]

TAMD allows for the description of longer time frame processes by increasing the temperature of the system during the trajectory calculation. This increases the speed at which certain processes will occur, such as conformational changes and bond

breakages.[76-77] In the case of this study, it increases the speed of geometry changes and bond breakages. There have been current studies into the pyrolysis of cellobiose and maltose *via* CPMD that confirm the viability of this methodology using thermogravimetric and mass spectroscopic experiments.[75] Caution should be used while using this methodology because if a temperature that is selected is too high, energetically forbidden states can be accessed. Alongside energetically forbidden states, the addition of too much energy can also further the system from the BO potential energy surface.[76-77]

To describe the kinetic energy of the nuclei during these TAMD trajectory calculations, the nuclear kinetic energy (NKE) must be specified. This allows for the immediate propagation of the kinetic energy responsible for the randomized velocities of the nuclei. This is important as both temperature and energy cannot be exactly conserved for these calculations. Once specified, NKE is then randomly dispersed throughout the system. In eq 17, N represents the number of nuclei in the system, k_B represents Boltzmann's constant, and T represents the desired temperature of the system.[79]

$$NKE = \frac{3}{2}(N-1)\,k_B T \tag{17}$$

CHAPTER 2: METHODOLOGY

2.1 Evaluated Methods

New Evaluated Model Chemistries. The thermochemical properties of bond dissociation pathways for methyl linoleate were computed with an eye towards direct chemical dynamics simulations. Therefore, economy of the method is a strong consideration along with accuracy. The B97-D [46,47], B3LYP [48], and M06-2X [49] density functionals were tested; additionally the wavefunction theory method MP2 [81] was included. Basis sets were also tested; 6-31G(d), 6-31+G(d,p), 6-311++G(2d,p), cc-pVDZ, and aug-cc-pVDZ [43] are discussed herein. All calculations were completed with the *Gaussian 09* suite. [85] Both geometry optimization and frequency analyses were performed in the gas phase. Frequency analysis allows for identification of the stationary points as minima or transition state structures, as well as providing zero-point vibrational energy (ZPVE).

The B97-D density functional is a hybrid meta-generalized gradient approximation (HGGA) constructed from Becke's 1997 exchange and correlation functionals with an additional semi-empirical dispersion correction factor of Grimme (G2).[46-47]

B3LYP was selected because it is a hyper-GGA DFT hybrid functional. B3LYP was parameterized against the G2 data base where it achieved an absolute error of 2.0 kcal/mol for describing atomization energies.[43, 45, 48] As mentioned earlier, B3LYP has been commonly employed in describing similar organic molecular systems. However, the

technical limitations of this functional prompt investigation into the viability of using B3LYP to describe methyl linoleate's thermochemical properties.

M06-2X was selected because it is a hyper-GGA DFT hybrid functionals commonly employed in describing organic molecular systems.[11, 14, 27-28, 43, 45, 49-51] Truhlar and Zhao had parameterized M06-2X specifically to describe the thermochemistry, kinetics, and noncovalent interactions of main-block elements.[11, 14, 49-51] Because of the ability to describe π-π interactions, hydrogen bonding, and other long-range forces, M06-2X has been recently used to describe bond dissociations in methyl linolenate (as opposed to this study's methyl linoleate).[14]

The perturbative second-order Møller-Plesset method (MP2; MBPT2) was included in testing due to its relative success in describing longer-range effects that may be important in molecules as large as methyl linoleate.[43, 45, 52] This method has been used in thermochemical calculations of main-block elements due to its accuracy in describing bond lengths, electron correlation, and geometry optimizations of minima. An additional advantage to using MP2 is that it is not size dependent (while the DFT methods herein are).[29, 43, 45, 52] There has also been literature published describing the thermal cracking of small hydrocarbons using the MP2/6-31G(d) method.[29]

Three Pople and two Dunning basis sets were chosen for evaluation for this study. While a larger basis set is more descriptive of the atomic orbitals used in constructing the wavefunctions of chemical systems, there seems to be precedent in recent literature to suggest using smaller basis sets when describing larger chemical systems.[11, 16, 20] To gauge this effect for our selected FAMEs, we have evaluated the Pople basis sets of 6-31G(d), 6-31+G(d,p) [82], and 6-311G++(2d,p) [83]. The Dunning cc-PVDZ and aug-cc-

pVDZ [84] basis sets were evaluated for how accurately they could describe our FAME chemical systems.

2.2 ADMP Parameterization

For ADMP trajectory calculations to accurately model the thermal cracking of methyl linoleate, certain parameters had to be selected and optimized. The parameters that were optimized include the description of the thermodynamics and the time scales of the system. Another parameter included the inclusion of a semi-empirical improvement of the description of the long-range forces of the system.

Temperature. The parameters governing the thermodynamics of the system can be reduced to two parameters: the accelerated temperature of the system and the use of a thermostat. The temperatures that were evaluated were 1000, 1500, 2000, 2250, 2500, 2750, 3500, 3750, and 4000 K. The logic behind these evaluations was to select the lowest temperature that would reliably result in bond dissociations within the selected timeframe of the trajectory calculation. If the temperature was too low, no bond dissociations would be observed. However, if the temperature is too high, energetically disfavored system states can be observed. The inclusion of a thermostat was also evaluated, which would allow the system to be treated as if it were subjected to a "heat bath". A thermostat in the trajectory calculation allows for the conservation of thermal energy of the system. The reasoning for this is that the kinetic and thermal energy for the trajectory calculations are not perfectly conserved, so without a thermostat the temperature of the system will begin to decrease with time.

Timeframe. The parameters governing the timeframes of the trajectory calculations include the step size and the overall number of time steps. The step sizes represent the change in time used for each step of the calculation. The step sizes that were evaluated were 0.1, 1.0, and 2.5 femtoseconds (fs). The advantage of using a small step size is the more physical treatment of bond vibrations during the trajectory calculations. However, this comes at the cost of overall timeframe size and computational cost. With a larger step size, you can describe a longer overall timeframe. This approach presents the risk of the unphysical treatment of vibrations in the form of nuclei entering one another. The total number of integration time steps that were evaluated were 2000, 2500, 4000, and 5000 steps. In conjunction with the aforementioned step sizes, the overall timeframe ranged from 200 fs to 12.5 picoseconds (ps) of simulated time.

Semi-Empirical Dispersion Correction. The parameter of including a semi-empirical dispersion correction was decided because of the need to describe long-range forces. Due to the programming of the ADMP code, duffuse basis functions cannot be used as they lead to linear dependencies that crash the code. To compensate for this loss, Grimme's third generation of semi-empirical dispersion correction was included. This allows for more accurate description of dispersion and π-π interaction forces, which is important for intermolecular forces and forces between thermally cracked fragments. Becke and Johnson's dispersion dampening correction factor was attempted for these ADMP trajectory calculations, but the code would not allow for its use.

CHAPTER 3: RESULTS AND DISCUSSION

3.1 Benchmark Studies

Homolytic Bond Cleavage of Exemplar Compounds. The primary mechanism of thermal cracking is dominated by homolytic bond scission. Therefore, the most effective method to describe the thermal cracking of FAMEs must be able to describe bond dissociation accurately. To evaluate the best method for describing bond dissociations, a list of reactions was compiled that have experimental BDE data.[53] These reactions (1 – 44, Chart 2) were chosen for structural resemblance to FAMEs (chemical moiety representatives; CMRs). The CMR reactions can be separated into different classes describing the bond breaking. Reactions 1 – 24 are carbon-hydrogen bond scissions, reactions 25 – 35 are carbon-carbon bond scissions, reactions 36 – 42 are mostly carbon-oxygen bond scissions, and reactions 43 – 44 are double bond scissions.

The BDEs were calculated for the CMR reactions 1 – 44 (Figure 7) and compared to experimentally determined values by computing the absolute percent deviation (APD) according to the following equation:

$$APD = \left|\frac{\Delta E_{calc} - \Delta H_{exp}}{\Delta H_{exp}}\right| \quad (18)$$

The mean APD (MAPD) was computed for the collection of CMR reactions 1 – 44 (Figure 7). These data appear in Table 1. Once all the absolute percent deviations were

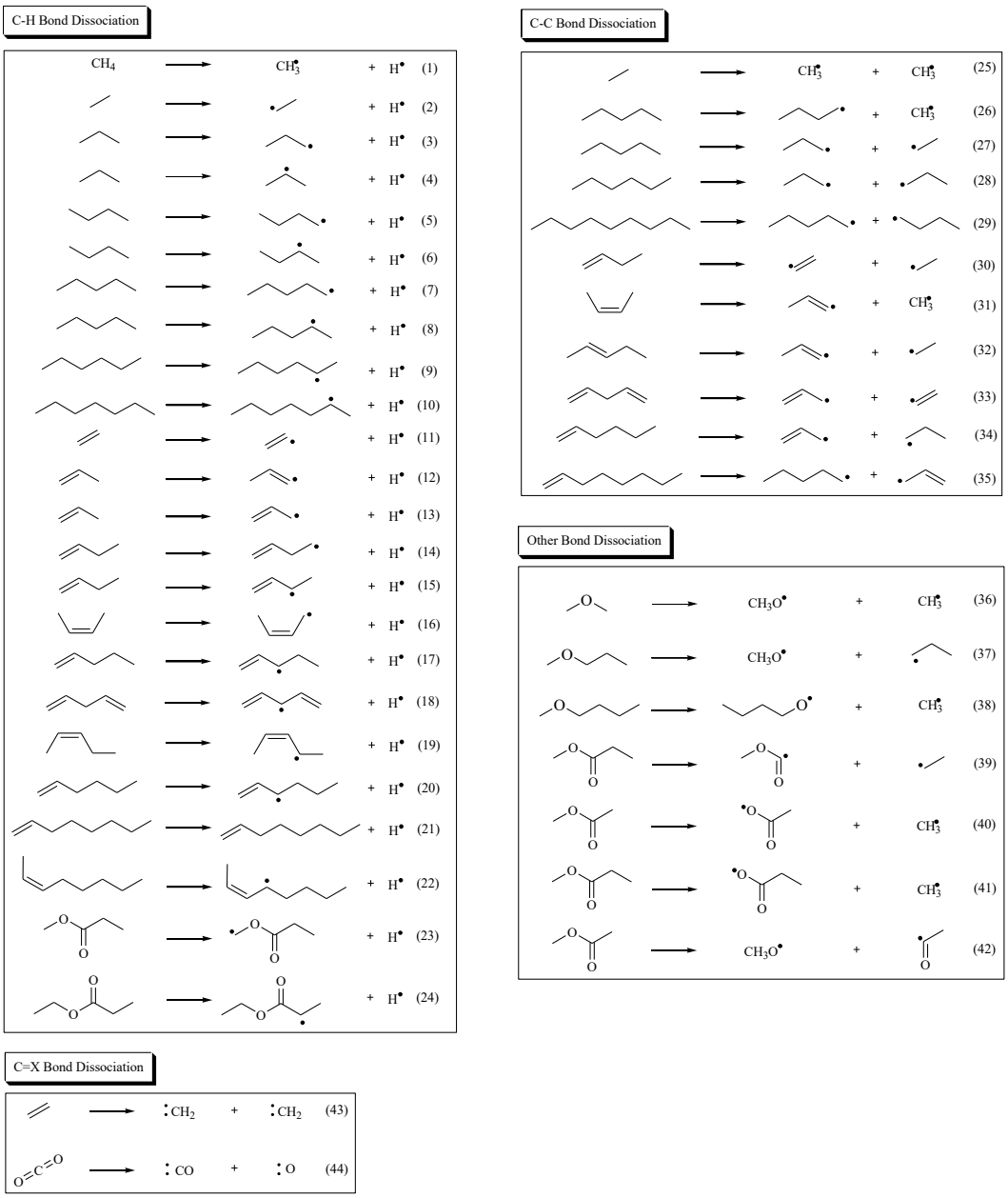

Figure 7. Chemical Moiety Representative (CMR) Reactions with Structural Resemblance to Fatty-Acid Methyl Esters (FAMEs) Methyl Linoleate and have Experimental Bond Dissociation Energies (BDEs) Reported.[53]

calculated for all of the methods, they were separated into their representative bond classes for evaluation. The absolute percent deviations were averaged for each bond class to find

TABLE 1. Mean Average Percent Deviations (MAPDs) in Calculated Homolytic Bond Dissociation Energies (BDEs) for Chemical Moiety Representative (CMR) Reactions 1 – 44.

	B3LYP	M06-2X	B97D	MP2	CBS-QB3
6-31G(d)	5.0%	3.1%	5.1%	6.4%	2.4%
6-31+G(d,p)	7.1%	2.8%	6.8%	5.3%	
6-311G++(2d,p)	7.9%	3.2%	7.8%	5.6%	
cc-PVDZ	7.1%	3.3%	6.9%	5.5%	
aug-cc-pVDZ	8.0%	3.3%	7.7%	6.0%	

TABLE 2. Mean Average Percent Deviations (MAPDs) in Calculated Homolytic Bond Dissociation Energies (BDEs) for Chemical Moiety Representative (CMR) Reactions 1 – 44 Separated by Bond Type.

C-H Bond Dissociation (Reactions 1 – 25, Figure 7)					
	B3LYP	M06-2X	B97D	MP2	CBS-QB3
6-31G(d)	3.0%	1.5%	2.8%	6.5%	1.4%
6-31+G(d,p)	3.1%	1.7%	2.7%	4.6%	
6-311G++(2d,p)	4.2%	2.3%	4.3%	4.6%	
cc-PVDZ	4.8%	2.6%	4.8%	4.8%	
aug-cc-pVDZ	5.0%	3.0%	5.0%	4.9%	
C-C Bond Dissociation (Reactions 25 – 35, Figure 7)					
6-31G(d)	6.7%	4.5%	6.3%	7.4%	3.7%
6-31+G(d,p)	12.7%	3.3%	11.5%	6.6%	
6-311G++(2d,p)	13.4%	3.8%	11.7%	7.2%	
cc-PVDZ	10.4%	3.4%	8.7%	7.3%	
aug-cc-pVDZ	12.2%	3.1%	10.3%	8.2%	
Other Bond Dissociation (Reactions 36 – 42, Figure 7)					
6-31G(d)	9.3%	5.9%	10.5%	5.7%	3.4%
6-31+G(d,p)	12.8%	4.6%	13.6%	5.2%	
6-311G++(2d,p)	13.3%	4.8%	13.8%	6.3%	
cc-PVDZ	10.6%	5.2%	11.1%	4.6%	
aug-cc-pVDZ	12.8%	4.4%	13.1%	6.3%	
C=X Bond Dissociation (Reactions 43 – 44, Figure 7)					
6-31G(d)	1.5%	2.3%	3.8%	3.4%	0.1%
6-31+G(d,p)	3.0%	4.4%	3.1%	4.3%	
6-311G++(2d,p)	1.9%	3.3%	3.3%	2.3%	
cc-PVDZ	1.9%	3.1%	3.4%	4.8%	
aug-cc-pVDZ	2.6%	3.6%	3.2%	3.1%	

the mean absolute percent deviation (MAPD). The MAPDs were tabulated for each method for each bond class in Table 2.

Just as predicted earlier, B3LYP was found to not be an appropriate functional for this study. In every reaction, with the noted exception of reactions 18 and 19, M06-2X outperformed B3LYP in describing the energetics of homolytic bond cleavage. Similar cases of M06-2X outperforming B3LYP has been observed in other benchmark studies.[14, 27-28] The difference in MAPD describing homolytic bond cleavages between B3LYP and M06-2X was found to be as high as 9.8% in favor of M06-2X.

3.2 Bond Dissociation Studies

Homolytic Bond Cleavage of Methyl Linoleate. The bond dissociations of methyl linoleate were modeled using the M06-2X/6-31+G(d,p) method. Figure 8 shows the optimal geometry and the observed bond dissociations of methyl linoleate. The bis-allylic site on carbon 11 has a predictably low C-H BDE of 76.3 kcal/mol. However, this method also revealed other likely sites of bond dissociation present in methyl linoleate. Between carbons 7 and 8, the BDE was calculated to be 74.0 kcal/mol. Between carbons 14 and 15, the BDE was calculated to be 72.4 kcal/mol. Together, these three sites represent the most energetically-favored sites of homolytic bond cleavage in methyl linoleate.

These energetically favored sites of homolytic bond scission have been predicted in earlier literature, but while using the B3LYP/6-31G(d,p) method.[16, 20] For the C-H bis-allylic site on carbon 11, the BDE was predicted to be 70 kcal/mol, where this study

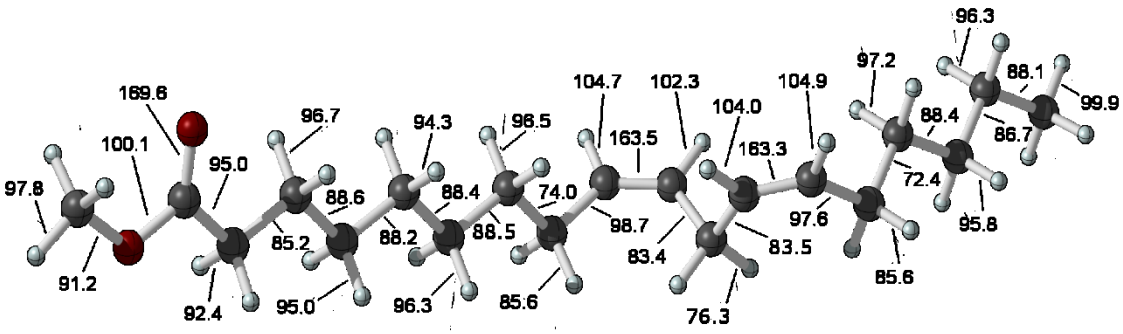

FIGURE 8. M06-2X/6-31+G(d,p) optimized structure. BDEs displayed in kcal/mol

predicts 76.3 kcal/mol. For the homolytic bond scission of carbons 7 and 8, the BDE was predicted to be 70 kcal/mol, whereas this study predicts 74.0 kcal/mol. Between carbons 14 and 15, the BDE was predicted by the B3LYP/6-31G(d,p) method to be 70 kcal/mol compared to the 72.4 kcal/mol presented in this study.[20] The discrepancy could be explained by B3LYP's overestimation of the stabilization effects of conjugated π-bonded segment of methyl linoleate, as well as the lack of diffuse functions when describing heavy atoms.[38-43, 45]

3.3 ADMP Trajectory Studies

Parameterization. The main parameters that were tested for this study were temperature, timeframe, and use of Grimme's semi-empirical dispersion correction. These parameterization trajectory calculations were to validate the method to be used for the rest of this study to model the thermal cracking of methyl linoleate. In turn, we intend to extend the use of these parameters for the future studies of other FAME compounds during the thermal cracking process.

As previously mentioned, The temperatures that were evaluated to model the thermal cracking process were 1000, 1500, 2000, 2250, 2500, 2750, 3500, 3750, and 4000 K. Temperatures 1000, 1500, 2000, 2250, 2500, 2750, and 3000 K did not produce bond scissions in the allotted timeframes of 250-500 fs. 3500 K was the first temperature that had observed bond scissions. Figure 9 demonstrates the naming scheme of the atoms in methyl linoleate.

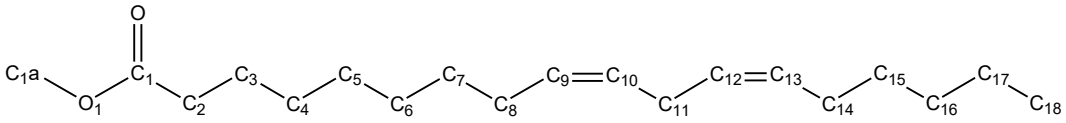

FIGURE 9. Atomic naming scheme to describe bond scissions during the thermal cracking of methyl linoleate.

The first temperature to yield a bond dissociation was 3500 K. The bond dissociations observed, the time of occurrence, and the overall timeframe of the trajectory are presented in Figure 10. The products generated were commodity ester compounds, carbon dioxide, natural gas, gasoline and kerosene products. The production of gasoline and kerosene sized hydrocarbons reflect similar products determined by GC and HPLC on the products of thermal cracking experiments. [19, 80] There were 7 trajectories at 3500 K that only yielded conformational changes in methyl linoleate. Due to these unreactive trajectories, higher temperatures were attempted.

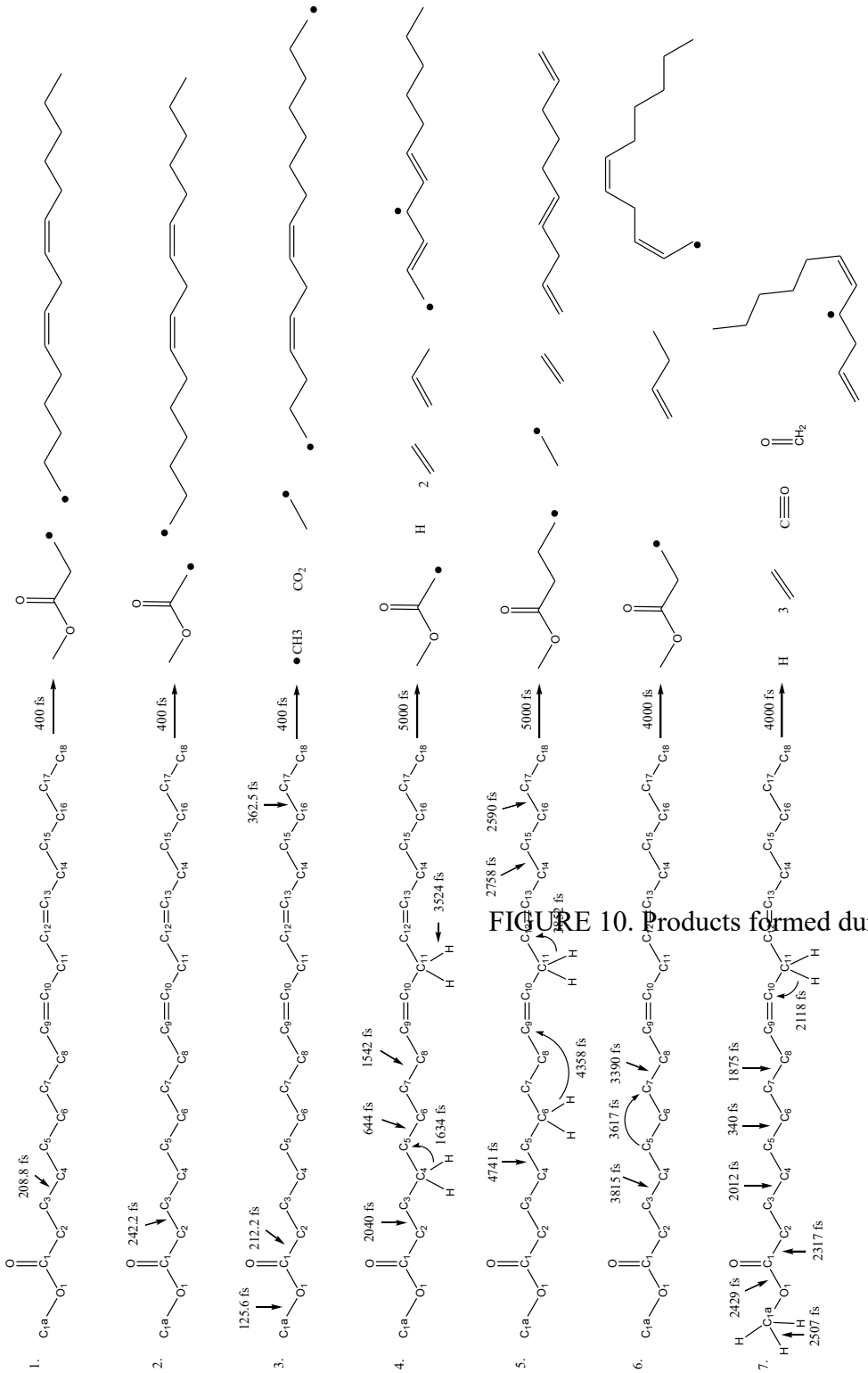

FIGURE 10. Products formed during parameterization trajecto

Figure 11 outlines the result of the trajectory parameterized to 3750 K. The 3750 K trajectory yielded bond scissions at C14-C15 (80.0 fs) and C17-C18 (193.6 fs). This yielded the products of a methyl radical, a cyclopropane, and a 9,11-tetradecadien-14-yl radical. Due to the success of this trajectory, a higher temperature parameter was evaluated.

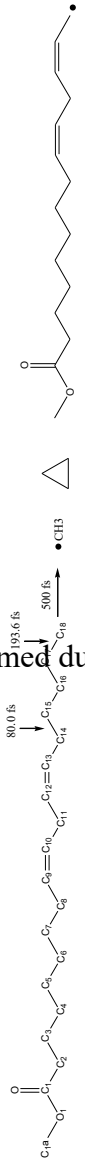

FIGURE 11. Products formed during parameterization trajectories at 3750 K

4000 K trajectories produced the most bond scissions. Of these, trajectory 4 produced the most bond scissions. The fourth trajectory produced bond scissions at C11-C12 (1528 fs), C13-C14 (1541 fs), C7-C8 (1648 fs), C5-C6 (1756 fs), C15-C16 (1845 fs), C3-C4 (2056), C17-C18 (3471 fs), C1-C2 (3783 fs), C1-O1 (4329 fs), and C1a-H1 (4437 fs). This fourth trajectory formed a methyl radical, a hydrogen atom, 1,3-butadiene, acetylene, carbon monoxide, formaldehyde, and 5 molecules of ethylene. No further trajectories parameterized to 4000 K were attempted after trajectory 4.

The standard time step for ADMP trajectories in *Gaussian 09* is set to 0.1 fs. A quantum mechanics insight was used to rationalize a larger step size. A C-H bond vibration (which represents the fastest bond vibration in most FAMEs), occurs at 3000 wavenumbers (cm^{-1}). When converted into fs, it is equal to a vibrational frequency of approximately 11 fs. We need a step size an order of magnitude smaller than 11 fs in order to prevent unphysical representations of the bond vibrations. To allow for larger timeframes, we tested 0.1, 0.5, 1.0, and 2.5 fs time steps. Up to 1.0 fs performed well in describing the bond vibrations of our system. However, the 2.5 fs time step could never finish a trajectory successfully due to convergence errors and other technical issues related to unphysical atom interactions.

Production Data. For the production trajectories, 3500 K was selected as the most appropriate temperature to describe the thermal cracking process. This was because it was the first temperature that had observed bond scissions. The ratios of bond breakages per 1000 picoseconds was determined to be 2.5 for 3500 K, 4.0 for 3750 K, and 4.0 for 4000 K. The higher temperatures were ultimately not considered because of the high levels of bond breakages and high-energy products observed during the thermal

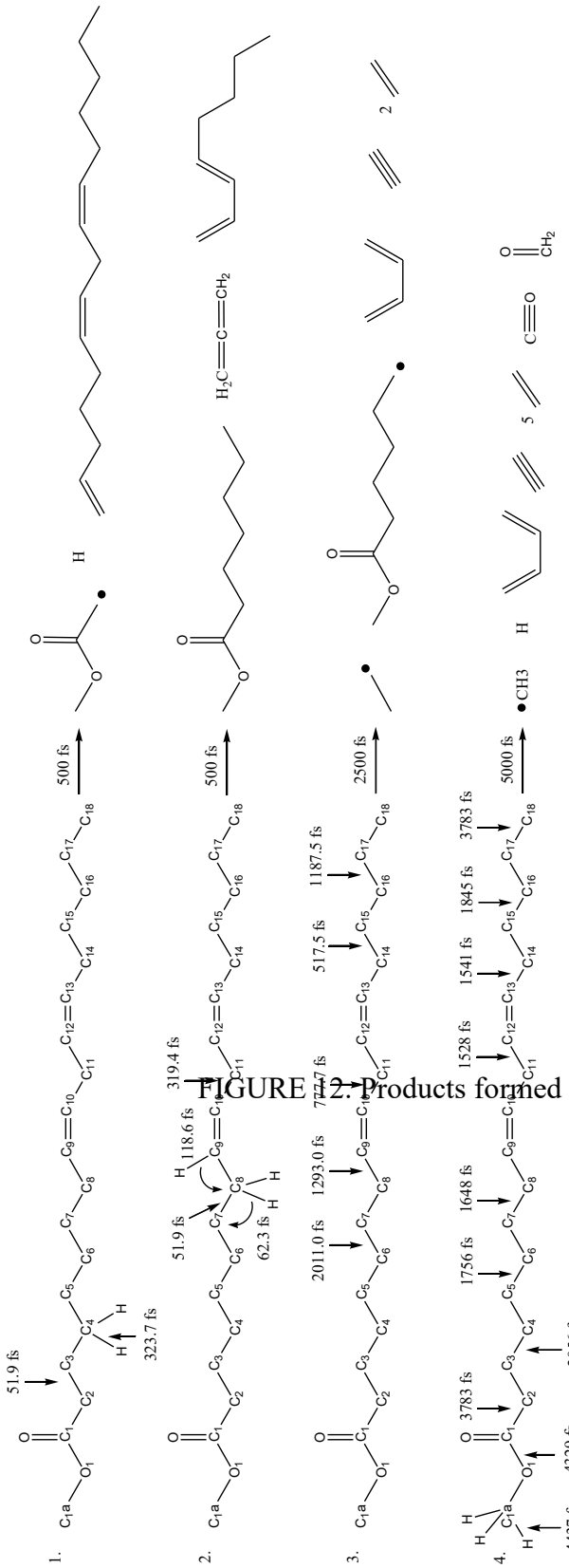

FIGURE 12. Products formed during parameterization trajectories a

cracking process. In trajectory 4 of the 4000 K parameterization trajectories, methyl linoleate was completely gasified with the exception of 1,3-butadiene and formaldehyde. Despite the fact that this trajectory represents a random sampling of the possible energy states of the thermal cracking of methyl linoleate, 4000 K represented an energy state that was determined to be too high to describe the thermal cracking process accurately. In turn, 3750 K was decided against to minimize the appearance of forbidden energy states as 3500 K has been proven capable of describing bond dissociations of methyl linoleate during a reasonable timeframe.

Upon initial inspection, it was decided that 5000 fs represented the largest timeframe for a trajectory to be calculated within a reasonable time with our current computational cluster. However, due to the time-consuming nature of the ADMP trajectory calculations, it was decided to enact a "divide and conquer" approach to the trajectories. Because many bond dissociations occur at under 2000 fs, it was decided to have the "initial" trajectory occupy this timeframe. Any products formed within this time would be separated into their own "branch" trajectory as to cut down on computational cost. This could also allow for the circumstantial increase of the overall timeframe of the "total" trajectory as further branched trajectories were to be conducted for each new thermally cracked product. The branch trajectories would ultimately conclude when no new products are formed.

This requires the export of the initial velocity vectors for each atom to the appropriate branch trajectory from the end of the initial trajectory. However, due to time constraints, this portion was not possible to conduct for this study.

The inclusion of Grimme's GD3 semi-empirical dispersion was decided upon to allow for the more accurate depiction of long-range forces present during the thermal cracking process. The inclusion of GD3 did not produce any unphysical results. However, the effect was not strong enough to cause intermolecular combination reactions between the thermally cracked products within the observed trajectories at this point.

The results of the initial production trajectories with observed bond scissions are presented in Figure 13. The main products thus far are commodity ester, natural gas, and a kerosene compound. In order to get a fair distribution of products, 100 trajectories must be completed. Figure 13 only represents our 5 productive trajectories out of 12 total trajectories currently attempted with our current methodology. Further work will be conducted in the future to continue this study.

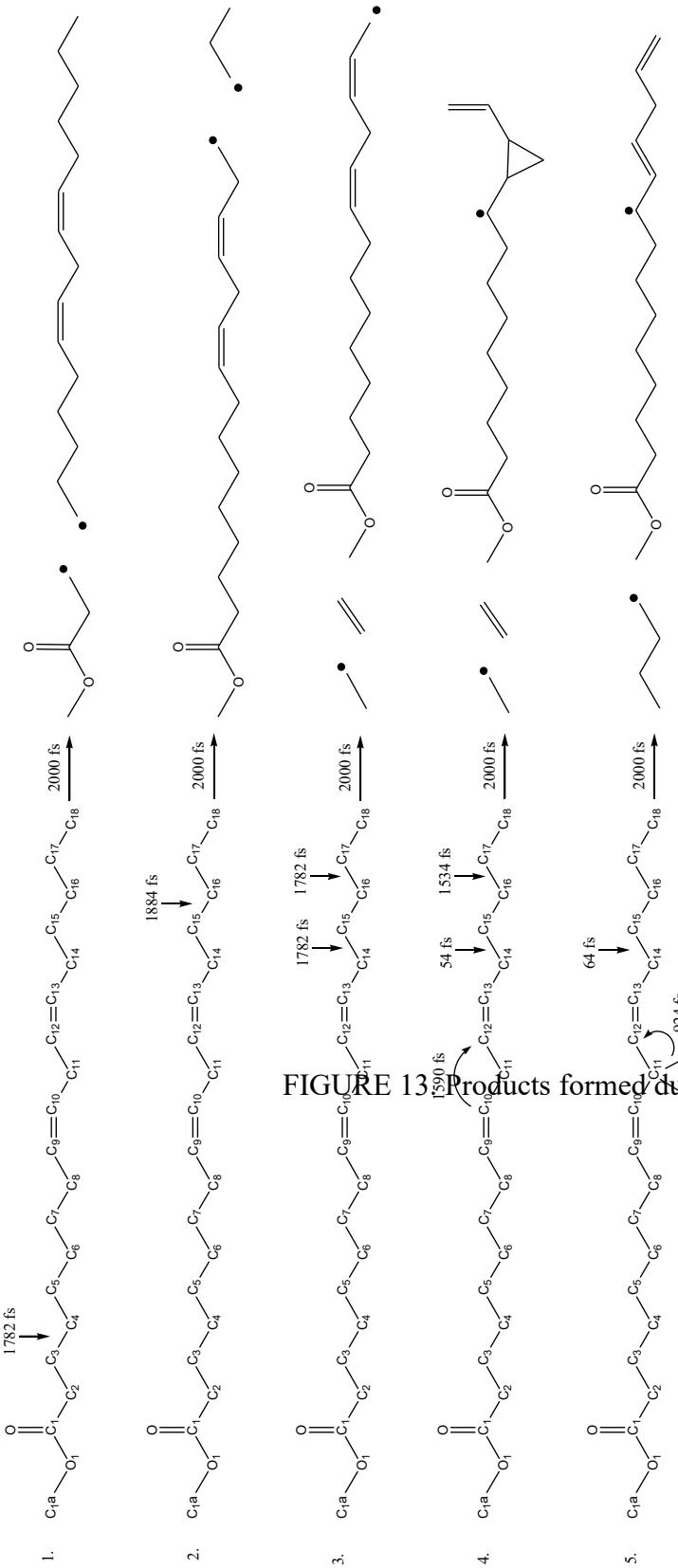

FIGURE 13. Products formed during productive production traje

CHAPTER 4: SUMMARY AND CONCLUSIONS

To better describe the thermal cracking process, ADMP trajectory calculations were employed. To use the ADMP method, an appropriate model chemistry must be used. The most appropriate model chemistry was selected by comparing calculated BDEs to experimentally determined BDEs. This model chemistry was determined to be M06-2X/6-31+G(d,p).

Once the model chemistry was selected, the parameters of the ADMP trajectory calculations had to be determined. Parameterization trajectories were used to determine the appropriate timeframe, temperature, and presence of a semi-empirical dispersion correction factor GD3. The selected parameters for the production trajectories were the time step of 1.0 fs with an overall timeframe of 2000 fs, GD3 dispersion correction, and the temperature 3500 K. Currently, this project is ongoing.

A promising new method describing the thermal cracking of FAMEs has been discovered. Despite the relatively few trajectories currently completed, the results are promising. Earlier parameterization trajectories have produced realistic products. With the continuation of the production trajectories, a more detailed description of the products formed during the thermal cracking process of methyl linoleate can be made.

This *ab initio* approach to the description of the thermal cracking process should allow for a more accurate and detailed description than methods proposed in the past. The strengths of this method lie in the atomic-level description of the FAME system as time progresses, and the *ab initio* treatment of the trajectories allow the flexibility to analyze many species of FAMEs for future analysis of the thermal cracking process.

REFERENCES

1. Aboim, J. B.; Oliveira, D.; Ferreira, J. E.; Siqueira, A. S.; Dall'Agnol, L. T.; Rocha Filho, G. N.; Gonçalves, E. C.; Nascimento, L. A., Determination of biodiesel properties based on a fatty acid profile of eight Amazon cyanobacterial strains grown in two different culture media. *RSC Adv.* **2016,** *6* (111), 109751-109758.

2. Augustine, C. In *A COMPARISON OF GEOTHERMAL WITH OIL AND GAS WELL DRILLING COSTS*.

3. Demirbas, A., *Biodiesel: A Realistic Fuel Alternative for Diesel Engines*. Springer: London, 2008; p 213.

4. Fagan, M. N., Resource Depletion and Technical Change: Effects on U.S. Crude Oil Finding Costs from 1977 to 1994. *The Energy Journal* **1997,** *18* (4), 91-105.

5. Fukuda, H.; Kondo, A.; Noda, H., Biodiesel fuel production by transesterification of oils. *Journal of Bioscience and Bioengineering* **2001,** *92* (5), 405-416.

6. Hannon, M.; Gimpel, J.; Tran, M.; Rasala, B.; Mayfield, S., Biofuels from algae: challenges and potential. *Biofuels* **2010,** *1* (5), 763-784.

7. Patil, P. D.; Gude, V. G.; Reddy, H. K.; Muppaneni, T.; Deng, S., Biodiesel Production from Waste Cooking Oil Using Sulfuric Acid and Microwave Irradiation Processes. *Journal of Environmental Protection* **2012,** *03* (01), 107-113.

8. Pogaku, R.; Raman, J. K.; Ravikumar, G., Evaluation of Activation Energy and Thermodynamic Properties of Enzyme-Catalysed Transesterification Reactions. *Advances in Chemical Engineering and Science* **2012,** *02* (01), 150-154.

9. S., D. D.; M., D. M., Biodiesel Production From Animal Fats And Its Impact On The Diesel Engine With Ethanol-Diesel Blends: A Review. *International Journal of Emerging Technology and Advanced Engineering* **2012,** *2* (10), 179.

10. Sheehan, J.; Camobreco, V.; Duffield, J.; Graboski, M.; Shapouri, H., An Overview of Biodiesel and Petroleum Diesel Life Cycles. Agriculture, U. S. D. o.; Energy, U. S. D. o., Eds. Golden, CO, 1998; p 60.

11. Wang, M.; Liu, C.; Xu, X.; Li, Q., Theoretical study of the pyrolysis of vanillin as a model of secondary lignin pyrolysis. *Chemical Physics Letters* **2016,** *654*, 41-45.

12. Knothe, G., "Designer" Biodiesel: Optimizing Fatty Ester Composition to Improve Fuel Properties†. *Energy & Fuels* **2008,** *22* (2), 1358-1364.

13. Knothe, G.; Steidley, K. R., A comparison of used cooking oils: a very heterogeneous feedstock for biodiesel. *Bioresour Technol* **2009,** *100* (23), 5796-801.

14. Li, X.; Xu, X.; You, X.; Truhlar, D. G., Benchmark Calculations for Bond Dissociation Enthalpies of Unsaturated Methyl Esters and the Bond Dissociation Enthalpies of Methyl Linolenate. *The journal of physical chemistry. A* **2016,** *120* (23), 4025-36.

15. Moser, B. R., Influence of Blending Canola, Palm, Soybean, and Sunflower Oil Methyl Esters on Fuel Properties of Biodiesel†. *Energy & Fuels* **2008,** *22* (6), 4301-4306.

16. Osmont, A.; Catoire, L.; Gökalp, I.; Swihart, M. T., Thermochemistry of C−C and C−H Bond Breaking in Fatty Acid Methyl Esters. *Energy & Fuels* **2007,** *21* (4), 2027-2032.

17. Oyeyemi, V. B.; Keith, J. A.; Carter, E. A., Accurate Bond Energies of Biodiesel Methyl Esters from Multireference Averaged Coupled-Pair Functional Calculations. *The Journal of Physical Chemistry A* **2014,** *118* (35), 7392-7403.

18. Sawangkeaw, R.; Bunyakiat, K.; Ngamprasertsith, S., A review of laboratory-scale research on lipid conversion to biodiesel with supercritical methanol (2001–2009). *The Journal of Supercritical Fluids* **2010,** *55* (1), 1-13.

19. Luo, Y.; Ahmed, I.; Kubátová, A.; Šťávová, J.; Aulich, T.; Sadrameli, S. M.; Seames, W. S., The thermal cracking of soybean/canola oils and their methyl esters. *Fuel Processing Technology* **2010,** *91* (6), 613-617.

20. Osmont, A.; Catoire, L.; Dagaut, P., Thermodynamic data for the modeling of the thermal decomposition of biodiesel. 1. Saturated and monounsaturated FAMEs. *The journal of physical chemistry. A* **2010,** *114* (11), 3788-95.

21. Osmont, A.; Yahyaoui, M.; Catoire, L.; Gökalp, I.; Swihart, M. T., Thermochemistry of CO, (CO)O, and (CO)C bond breaking in fatty acid methyl esters. *Combustion and Flame* **2008,** *155* (1-2), 334-342.

22. Zhang, Y.; Wang, X.; Li, Q.; Yang, R.; Li, C., A ReaxFF Molecular Dynamics Study of the Pyrolysis Mechanism of Oleic-type Triglycerides. *Energy & Fuels* **2015,** *29* (8), 5056-5068.

23. D02.E0, S., *Standard Specification for Biodiesel Fuel Blend Stock (B100) for Middle Distillate Fuels*. ASTM International: West Conshohocken, PA, 2015.

24. Hu, Q.; Sommerfeld, M.; Jarvis, E.; Ghirardi, M.; Posewitz, M.; Seibert, M.; Darzins, A., Microalgal triacylglycerols as feedstocks for biofuel production: perspectives and advances. *Plant J* **2008,** *54* (4), 621-39.

25. Zhang, Z.; Yan, K.; Zhang, J., ReaxFF molecular dynamics simulations of the initial pyrolysis mechanism of unsaturated triglyceride. *Journal of Molecular Modeling* **2014,** *20* (3), 2127.

26. D02.07, S., *Standard Test Method for Pour Point of Petroleum Products*. ASTM International: West Conshohocken, PA, 2005.

27. Beste, A.; Buchanan, A. C., Computational Study of Bond Dissociation Enthalpies for Lignin Model Compounds. Substituent Effects in Phenethyl Phenyl Ethers. *The Journal of organic chemistry* **2009,** *74* (7), 2837-2841.

28. Kim, S.; Chmely, S. C.; Nimlos, M. R.; Bomble, Y. J.; Foust, T. D.; Paton, R. S.; Beckham, G. T., Computational Study of Bond Dissociation Enthalpies for a Large Range of Native and Modified Lignins. *The Journal of Physical Chemistry Letters* **2011,** *2* (22), 2846-2852.

29. Xiao, Y.; Longo, J. M.; Hieshima, G. B.; Hill, R. J., Understanding the Kinetics and Mechanisms of Hydrocarbon Thermal Cracking: AnAb InitioApproach†. *Industrial & Engineering Chemistry Research* **1997,** *36* (10), 4033-4040.

30. Rueda-Velásquez, R. I.; Gray, M. R., Monte Carlo Simulation of Asphaltenes and Products from Thermal Cracking. *Energy & Fuels* **2014,** *28* (4), 2352-2364.

31. Sundaram, K. M.; Froment, G. F., Modeling of Thermal Cracking Kinetics. 3. Radical Mechanisms for the Pyrolysis of Simple Paraffins, Olefins, and Their Mixtures. *Industrial & Engineering Chemistry Fundamentals* **1978,** *17* (3), 174-182.

32. van Duin, A. C. T.; Dasgupta, S.; Lorant, F.; Goddard, W. A., ReaxFF: A Reactive Force Field for Hydrocarbons. *The Journal of Physical Chemistry A* **2001,** *105* (41), 9396-9409.

33. Blanksby, S. J.; Ellison, G. B., Bond Dissociation Energies of Organic Molecules. *Accounts of chemical research* **2003,** *36* (4), 255-263.

34. de Almeida, N. E. C.; de Aguiar, I.; de Zawadzki, A.; Cardoso, D. R., Kinetics and Thermodynamics of 1-Hydroxyethyl Radical Reaction with Unsaturated Lipids and Prenylflavonoids. *The Journal of Physical Chemistry B* **2014,** *118* (49), 14278-14287.

35. Dong, X.; Fan, X.; Fan, Y.; Wen, Y., Reactive molecular dynamics simulation of the pyrolysis and combustion of benzene: ultrahigh temperature and oxygen-induced enhancement of initiation pathways and their effect on carbon black generation. *RSC Advances* **2015,** *5* (54), 43695-43704.

36. Hu, X.; Li, H.; Wu, T., Approaching and Bond Breaking Energies in the C−H Activation and Their Application in Catalyst Design. *The Journal of Physical Chemistry A* **2011,** *115* (5), 904-910.

37. Weismiller, M. R.; Duin, A. C. T. v.; Lee, J.; Yetter, R. A., ReaxFF Reactive Force Field Development and Applications for Molecular Dynamics Simulations of Ammonia Borane Dehydrogenation and Combustion. *The Journal of Physical Chemistry A* **2010,** *114* (17), 5485-5492.

38. Bartell, L. S., The correct physical basis of protobranching stabilization. *The Journal of Physical Chemistry A* **2012,** *116* (42), 10460-2.

39. Johnson, E. R.; Contreras-Garcia, J.; Yang, W., Density-Functional Errors in Alkanes: A Real-Space Perspective. *Journal of Chemical Theory and Computation* **2012,** *8* (8), 2676-81.

40. McKee, W. C.; Schleyer, P., Correlation effects on the relative stabilities of alkanes. *Journal of the American Chemical Society* **2013,** *135* (35), 13008-14.

41. Wodrich, M. D.; Corminboeuf, C.; Schleyer, P. v. R., Systematic Errors in Computed Alkane Energies Using B3LYP and Other Popular DFT Functionals. *Organic Letters* **2006,** *8* (17), 3631-3634.

42. Wodrich, M. D.; Wannere, C. S.; Mo, Y.; Jarowski, P. D.; Houk, K. N.; Schleyer, P. v. R., The Concept of Protobranching and Its Many Paradigm Shifting Implications for Energy Evaluations. *Chemistry: A European Journal* **2007,** *13* (27), 7731-7744.

43. Koch, W.; Holthausen, M. C., *A Chemist's Guide to Density Functional Theory*. 2nd ed.; Wiley-VCH: Weinheim, 2001.

44. Siebert, M. R.; Zhang, J.; Addepalli, S. V.; Tantillo, D. J.; Hase, W. L., The Need for Enzymatic Steering in Abietic Acid Biosynthesis: Gas-Phase Chemical Dynamics Simulations of Carbocation Rearrangements on a Bifurcating Potential Energy Surface. *Journal of the American Chemical Society* **2011,** *133* (21), 8335-8343.

45. Tsuneda, T., *Density Functional Theory in Quantum Chemistry*. Springer: Tokyo, 2014; p 207.

46. Grimme, S., Semiempirical GGA-type density functional constructed with a long-range dispersion correction. *Journal of Computational Chemistry* **2006,** *27* (15), 1787-1799.

47. Grimme, S.; Antony, J.; Ehrlich, S.; Krieg, H., A consistent and accurate ab initio parametrization of density functional dispersion correction (DFT-D) for the 94 elements H-Pu. *The Journal of Chemical Physics* **2010,** *132* (15), 154104.

48. Becke, A. D., Density-functional thermochemistry. III. The role of exact exchange. *The Journal of Chemical Physics* **1993,** *98* (7), 5648-5652.

49. Zhao, Y.; Truhlar, D., The M06 suite of density functionals for main group thermochemistry, thermochemical kinetics, noncovalent interactions, excited states, and transition elements: two new functionals and systematic testing of four M06-class functionals and 12 other functionals. *Theoretical Chemistry Accounts* **2008,** *120* (1-3), 215-241.

50. Zhao, Y.; Truhlar, D. G., Density Functionals with Broad Applicability in Chemistry. *Accounts of chemical research* **2008,** *41* (2), 157-167.

51. Zhao, Y.; Truhlar, D. G., How Well Can New-Generation Density Functionals Describe the Energetics of Bond-Dissociation Reactions Producing Radicals? *The Journal of Physical Chemistry A* **2008,** *112* (6), 1095-1099.

52. Head-Gordon, M.; Pople, J. A.; Frisch, M. J., MP2 energy evaluation by direct methods. *Chemical Physics Letters* **1988,** *153* (6), 503-506.

53. Luo, Y.-R., *Handbook of Bond Dissociation Energies in Organic Compounds*. CRC Press: Boca Raton, 2003.

54. Guvench, Olgun; MacKerell Alexander D.; Vanommeslaeghe, Kenno. Molecular Mechanics. *Current pharmaceutical design*. **2014**, 20, 20 3281–3292. https://www.ncbi.nlm.nih.gov/pmc/articles/PMC4026342/

55. Allen, Michael P. Computational Soft Matter: From Synthetic Polymers to Proteins. *NIC Series*. John von Neumann Institute for Computing, Julich. **2004**, 23, 1-28.

56. Porta, Felipe A. La; Ramalho, Teodorico C.; Santiago, Regis T.; Rocha, Marcus V. J.; da Cunha, Elaine F. F. Orbital Signatures as a Descriptor of Regioselectivity and Chemical Reactivity: The Role of the Frontier Orbitals on 1,3-Dipolar Cycloadditions. *J. Phys. Chem. A*. **2011**, 115, 824–833.

57. Kuhne, Thomas D.; Krack, Matthias; Mohamed, Fawzi R.; Parrinello, Michele. An Efficient and Accurate Car-Parrinello-like Approach to Born-Oppenheimer Molecular Dynamics. *Phys. Rev. Lett*. **2007**, 98.

58. Martínez, Enrique; Cawkwell, Marc J.; Voter, Arthur F.; Niklasson, Anders M. N. Thermostating extended Lagrangian Born-Oppenheimer molecular dynamics. *E Journ. of Chem. Phys*. **2015**, 142, 154120.

59. Marx, Dominik; Hutter, Jürg. *Ab Initio* Molecular Dynamics: Basic Theory and Advanced Methods. Cambridge University Press 2009.

60. P. Pulay. Molecular Physics: An International Journal at the Interface between Chemistry and Physics. *Molecular Phys*. **1969**, 17, 2, 197-204.

61. Feynman, R. P. Forces in Molecules. *Phys. Rev*. **1939**, 56, 340.

62. Esteve, J. G.; Falceto, Fernando; Cana, C. García. Generalization of the Hellmann-Feynman theorem. *Physics Letters A*. **2010**, 374, 6, 819-82.

63. Iyengar, Srinivasan S.; Schlegel, H. Bernhard; Voth, Gregory A. Atom-Centered Density Matrix Propagation (ADMP): Generalizations Using Bohmian Mechanics. *J. Phys. Chem. A*. **2003,** *107,* 7269-7277.

64. Schlegel, H. Bernhard; Millam, John M.; Iyengar, Srinivasan S; Voth, Gregory A.; Daniels, Andrew D.; Scuseria, Gustavo E.; Frisch, Michael J. *Ab initio* molecular dynamics: Propagating the density matrix with Gaussian orbitals. *Journ. of Chem. Phys*. **2001**. 114, 22.

65. Schlegel, H. Bernhard; Iyengar, Srinivasan S.; Li, Xiaosong; Millam, John M.; Voth, Gregory A.; Scuseria, Gustavo E.; Frisch, Michael J. *Ab initio* molecular dynamics: Propagating the density matrix with Gaussian orbitals. III. Comparison with Born–Oppenheimer dynamics. *Journ. of Chem. Phys*. **2002**, 117, 8694.

66. Joubert, Laurent; Adamo, Carlo. Static and dynamic descriptions of bond breaking/formation: A complementary view? *Journ. of Chem. Phys*. **2005**, 123, 211103.

67. Martínez, Enrique; Cawkwell, Marc J.; Voter, Arthur F.; Niklasson, Anders M. N. Thermostating extended Lagrangian Born-Oppenheimer molecular dynamics. *Journ. of Chem. Phys*. **2015**, 142, 154120.

68. El-Khoury, Patrick Z.; Bylaska, Eric J.; Hess, Wayne P. Time domain simulations of chemical bonding effects in surface-enhanced spectroscopy. *J. Chem. Phys.* **2013**, 139, 174303.

69. Rega, Nadia; Iyengar, Srinivasan S.; Voth, Gregory A.; Schlegel, H. Bernhard; Vreven, Thom; Frisch, Michael J. Hybrid Ab-Initio/Empirical Molecular Dynamics: Combining the ONIOM Scheme with the Atom-Centered Density Matrix Propagation (ADMP) Approach. *J. Phys. Chem. B* **2004,** 108, 4210-4220.

70. Hu, Xingbang; Li, Haoran; Wu, Tao. Approaching and Bond Breaking Energies in the C-H Activation and Their Application in Catalyst Design. *J. Phys. Chem. A*. **2011**, 115, 904–910.

71. Jay, Ashley N.; Daniel, Kelly A.; Patterson, Eric V. Atom-Centered Density Matrix Propagation Calculations on the Methyl Transfer from CH3Cl to NH3: Gas-Phase and Continuum-Solvated Trajectories. *J. Chem. Theory Comput.* **2007,** 3*,* 336-343.

72. Kroger, Jessica L.; Fried, Joel R.; Skelton, Adam A. Computational Simulations of Hydrolysis of Phosphazene Oligomer Utilizing Atom-Centered Density Matrix Propagation. *International Journal of Quantum Chemistry*. **2013**, 113, 63–70.

73. Deumens, E.; Diz, A.; Longo, R.; Ohrn, Y. Time-dependent theoretical treatments of the dynamics of electrons and nuclei in molecular systems. *Reviews of Modern Physics*. **1994**, 66, 3.

74. Tian, Wei Quan; Wang, Yan Alexander. Dynamics of the Staudinger Reaction. *J. Chem. Theory Comput.* **2005,** *1,* 353-362.

75. Murillo, Jessica D.; Moffet, Melissa; Biernacki, Joseph J.; Northrup, Scott. High-Temperature Molecular Dynamics Simulation of Cellobiose and Maltose. *AIChE Journal*. **2015**, 61, 8.

76. Ozer, Gungor; Valeev, Edward F.; Quirk, Stephen; Hernandez, Rigoberto. Adaptive Steered Molecular Dynamics of the Long-Distance Unfolding of Neuropeptide Y. *J. Chem. Theory Comput.* **2010,** *6,* 3026–3038.

77. Hu, Yue; Liu, Haiyan. Case Study on Temperature-Accelerated Molecular Dynamics Simulation of Ligand Dissociation: Inducer Dissociation from the Lac Repressor Protein. *J. Phys. Chem. A*. **2014**, 118, 9272−9279.

78. Bendt, Paul; Zunger, Alex. Simultaneous Relaxation of Nuclear Geometries and Electric Charge Densities in Electronic Structure Theories. *Physical Review Letters*. **1983**, 50, 21, 1684-1688.

79. Vimal, Deepali ; Pacheco, Alexander B.; Iyengar, Srinivasan S.; S. Stevens. Experimental and Ab Initio Dynamical Investigations of the Kinetics and Intramolecular Energy Transfer Mechanisms for the OH + 1,3-Butadiene Reaction between 263 and 423 K at Low Pressure. *The Journal of Physical Chemistry A* **2008** *112* (31), 7227-7237.

80. Kubátová, Alena; Šťávová, Jana; Seames, Wayne S.; Luo, Yan; Mojtaba, Sadrameli S.;, Linnen, Michael J.; Baglayeva, Ganna V.; Smoliakova, Irina P.; Kozliak, Evguenii I. Triacylglyceride Thermal Cracking: Pathways to Cyclic Hydrocarbons. *Energy Fuels* **2012**, 26, 672−685.

81. M. J. Frisch, M. Head-Gordon, and J. A. Pople, "Direct MP2 gradient method," *Chem. Phys. Lett.*, **166** (1990) 275-80.

82. R. Ditchfield, W. J. Hehre, and J. A. Pople, "Self-Consistent Molecular Orbital Methods. 9. Extended Gaussian-type basis for molecular-orbital studies of organic molecules," *J. Chem. Phys.*, **54** (1971) 724.

83. A. D. McLean and G. S. Chandler, "Contracted Gaussian-basis sets for molecular calculations. 1. 2nd row atoms, Z=11-18," *J. Chem. Phys.*, **72** (1980) 5639-48.

84. T. H. Dunning Jr., "Gaussian basis sets for use in correlated molecular calculations. I. The atoms boron through neon and hydrogen," *J. Chem. Phys.*, **90** (1989) 1007-23.

85. Frisch, M.J. *et al*. (2009). *Gaussian09*.Wallingford, CT, USA, Gaussian, Inc.

APPENDICES

Appendix A. B3LYP Benchmark Data.

Operator		B3LYP									
Basis Set		6-31G(d)		6-31+G(d,p)		6-311G++(2d,p)		cc-PVDZ		aug-cc-pVDZ	
Reaction #	Literature B.D.E (Kcal/mol)	Calculated B.D.E (Kcal/mol)	% Error	Calculated B.D.E (Kcal/mol)	% Error	Calculated B.D.E (Kcal/mol)	% Error	Calculated B.D.E (Kcal/mol)	% Error	Calculated B.D.E (Kcal/mol)	% Error
1	105.0	103.177	1.7%	102.628	2.3%	101.447	3.4%	101.072	3.7%	101.277	3.5%
2	100.5	98.326	2.2%	97.844	2.6%	96.614	3.9%	96.202	4.3%	96.562	3.9%
3	99.9	98.659	1.2%	98.142	1.8%	97.269	2.6%	96.982	2.9%	95.887	4.0%
4	98.1	94.334	3.8%	94.069	4.1%	92.837	5.4%	92.359	5.9%	92.929	5.3%
5	100.7	98.542	2.1%	98.064	2.6%	97.224	3.5%	96.932	3.7%	96.837	3.8%
6	98.3	94.583	3.8%	94.278	4.1%	93.055	5.3%	92.697	5.7%	93.180	5.2%
7	100.19	98.757	1.4%	98.280	1.9%	96.855	3.3%	96.834	3.4%	95.977	4.2%
8	99.21	94.535	4.7%	94.264	5.0%	92.992	6.3%	92.582	6.7%	92.286	7.0%
9	98.0	94.499	3.6%	94.229	3.8%	93.011	5.1%	92.627	5.5%	93.177	4.9%
10	98.0	94.492	3.6%	94.245	3.8%	92.992	5.1%	92.554	5.6%	93.173	4.9%
11	111.21	107.607	3.2%	107.864	3.0%	106.617	4.1%	105.834	4.8%	105.885	4.8%
12	111.1	108.488	2.4%	108.535	2.3%	107.339	3.4%	106.718	3.9%	107.465	3.3%
13	88.2	73.729	16.4%	83.624	5.2%	82.676	6.3%	81.904	7.1%	82.569	6.4%
14	98.1	98.823	0.7%	98.417	0.3%	97.205	0.9%	96.791	1.3%	97.213	0.9%
15	81.50	79.025	3.0%	79.456	2.5%	78.462	3.7%	77.498	4.9%	77.727	4.6%
16	85.3	80.130	6.1%	82.525	3.3%	81.543	4.4%	80.872	5.2%	81.478	4.5%
17	82.5	79.488	3.7%	79.884	3.2%	78.912	4.3%	78.068	5.4%	79.119	4.1%
18	76.60	68.519	10.6%	69.372	9.4%	68.560	10.5%	67.321	12.1%	67.751	11.6%
19	82.5	81.958	0.7%	82.261	0.3%	81.237	1.5%	80.346	2.6%	81.343	1.4%
20	83.4	80.628	3.3%	79.796	4.3%	78.839	5.5%	77.974	6.5%	79.065	5.2%
21	83.4	79.334	4.9%	79.781	4.3%	78.826	5.5%	77.943	6.5%	79.052	5.2%
22	81.9	78.584	4.0%	78.927	3.6%	81.904	0.0%	81.104	1.0%	77.310	5.6%
23	95.48	95.985	0.5%	95.704	0.2%	94.457	1.1%	94.722	0.8%	93.694	1.9%
24	95.60	93.066	2.7%	93.311	2.4%	92.030	3.7%	91.130	4.7%	91.431	4.4%
25	90.2	86.742	3.8%	82.819	8.2%	82.300	8.8%	85.237	5.5%	83.244	7.7%
26	88.79	84.284	5.1%	80.550	9.3%	79.987	9.9%	82.927	6.6%	81.208	8.5%
27	87.31	81.481	6.7%	77.882	10.8%	77.198	11.6%	80.080	8.3%	78.136	10.5%
28	87.50	82.226	6.0%	78.582	10.2%	77.901	11.0%	80.920	7.5%	78.469	10.3%
29	86.1	81.633	5.2%	78.023	9.4%	77.421	10.1%	80.228	6.8%	78.797	8.5%
30	100.0	97.385	2.6%	93.849	6.2%	89.837	10.2%	92.188	7.8%	94.303	5.7%
31	101.6	96.198	5.3%	92.542	8.9%	67.320	33.7%	69.888	31.2%	93.062	8.4%
32	99.81	92.836	7.0%	89.338	10.5%	88.655	11.2%	91.188	8.6%	89.873	10.0%
33	87.19	78.686	9.8%	75.966	12.9%	75.409	13.5%	77.414	11.2%	76.464	12.3%
34	75.00	66.674	11.1%	63.566	15.2%	63.094	15.9%	65.493	12.7%	63.926	14.8%
35	73.3	56.659	22.7%	63.430	13.5%	62.731	14.4%	64.998	11.3%	64.294	12.3%
36	83.1	76.933	7.4%	73.553	11.5%	73.207	11.9%	76.011	8.5%	73.227	11.9%
37	84.8	77.827	8.2%	74.408	12.3%	74.299	12.4%	77.194	9.0%	73.798	13.0%
38	84.4	75.650	10.4%	72.451	14.2%	72.718	13.8%	75.218	10.9%	73.053	13.4%
39	110.71	86.728	21.7%	84.259	23.9%	83.433	24.6%	85.409	22.9%	84.395	23.8%
40	84.30	79.284	5.9%	76.925	8.7%	76.313	9.5%	77.834	7.7%	76.824	8.9%
41	84.89	79.652	6.2%	77.195	9.1%	76.664	9.7%	78.323	7.7%	77.190	9.1%
42	100.50	92.928	7.5%	89.108	11.3%	88.422	12.0%	91.459	9.0%	88.420	12.0%
43	127.20	128.202	0.8%	124.822	1.9%	126.724	0.4%	126.762	0.3%	125.617	1.2%
44	174.09	170.071	2.3%	167.029	4.1%	167.976	3.5%	168.017	3.5%	167.167	4.0%

Appendix B. M06-2X Benchmark Data.

Operator		M06-2X									
Basis Set		6-31G(d)		6-31+G(d,p)		6-311G++(2d,p)		cc-PVDZ		aug-cc-pVDZ	
Reaction #	Literature B.D.E (Kcal/mol)	Calculated B.D.E (Kcal/mol)	% Error	Calculated B.D.E (Kcal/mol)	% Error	Calculated B.D.E (Kcal/mol)	% Error	Calculated B.D.E (Kcal/mol)	% Error	Calculated B.D.E (Kcal/mol)	% Error
1	105.0	103.798	1.1%	102.956	1.9%	102.082	2.8%	101.769	3.1%	101.585	3.3%
2	100.5	99.929	0.6%	99.104	1.4%	98.057	2.4%	97.770	2.7%	97.763	2.7%
3	99.9	100.074	0.2%	99.302	0.6%	98.309	1.6%	98.223	1.7%	97.803	2.1%
4	98.1	96.485	1.6%	95.961	2.2%	94.732	3.4%	94.317	3.9%	94.563	3.6%
5	100.7	100.659	0.0%	99.877	0.8%	98.686	2.0%	98.437	2.2%	98.461	2.2%
6	98.3	97.118	1.2%	96.565	1.8%	95.532	2.8%	95.065	3.3%	95.423	2.9%
7	100.19	99.795	0.4%	99.187	1.0%	97.943	2.2%	97.649	2.5%	96.863	3.3%
8	99.21	96.549	2.7%	96.055	3.2%	94.652	4.6%	94.262	5.0%	93.837	5.4%
9	98.0	96.730	1.3%	96.273	1.8%	95.539	2.5%	95.050	3.0%	94.986	3.1%
10	98.0	96.260	1.8%	95.792	2.3%	94.426	3.6%	94.027	4.1%	94.525	3.5%
11	111.21	108.265	2.6%	108.257	2.7%	107.242	3.6%	106.511	4.2%	106.379	4.3%
12	111.1	109.257	1.7%	109.102	1.8%	108.093	2.7%	107.474	3.3%	108.013	2.8%
13	88.2	87.166	1.2%	86.670	1.7%	85.903	2.6%	85.242	3.4%	85.434	3.1%
14	98.1	100.696	2.6%	99.963	1.9%	98.860	0.8%	98.446	0.4%	98.526	0.4%
15	81.50	83.190	2.1%	83.098	2.0%	82.317	1.0%	81.225	0.3%	81.171	0.4%
16	85.3	86.028	0.9%	85.362	0.1%	84.326	1.1%	84.019	1.5%	83.320	2.3%
17	82.5	83.564	1.3%	83.497	1.2%	82.630	0.2%	81.774	0.9%	82.395	0.1%
18	76.60	73.980	3.4%	74.287	3.0%	73.643	3.9%	72.370	5.5%	72.436	5.4%
19	82.5	85.416	3.5%	85.218	3.3%	84.204	2.1%	83.449	1.1%	84.068	1.9%
20	83.4	84.233	1.0%	83.949	0.7%	82.868	0.6%	81.898	1.8%	82.919	0.6%
21	83.4	83.427	0.0%	83.350	0.1%	82.451	1.1%	81.528	2.2%	82.167	1.5%
22	81.9	82.630	0.9%	82.314	0.5%	84.594	3.3%	84.019	2.6%	81.562	0.4%
23	95.48	98.155	2.8%	97.764	2.4%	96.920	1.5%	95.778	0.3%	95.517	0.0%
24	95.60	95.679	0.1%	95.444	0.2%	94.496	1.2%	93.597	2.1%	93.616	2.1%
25	90.2	92.627	2.7%	88.721	1.6%	88.244	2.2%	91.241	1.2%	89.257	1.0%
26	88.79	91.362	2.9%	87.702	1.2%	86.767	2.3%	89.687	1.0%	87.993	0.9%
27	87.31	90.197	3.3%	86.670	0.7%	85.472	2.1%	88.423	1.3%	86.937	0.4%
28	87.50	91.365	4.4%	87.873	0.4%	86.954	0.6%	90.084	3.0%	88.570	1.2%
29	86.1	90.527	5.1%	86.935	1.0%	85.607	0.6%	88.486	2.8%	87.203	1.3%
30	100.0	105.574	5.6%	102.075	2.1%	97.142	2.9%	99.248	0.8%	102.528	2.5%
31	101.6	102.509	0.9%	99.047	2.5%	76.127	25.1%	78.810	22.4%	99.664	1.9%
32	99.81	100.418	0.6%	97.141	2.7%	96.110	3.7%	98.639	1.2%	97.761	2.1%
33	87.19	88.005	0.9%	85.247	2.2%	84.612	3.0%	86.426	0.9%	85.717	1.7%
34	75.00	77.620	3.5%	74.385	0.8%	73.764	1.6%	76.025	1.4%	74.972	0.0%
35	73.3	77.247	5.4%	73.916	0.8%	73.331	0.0%	75.441	2.9%	74.706	1.9%
36	83.1	85.525	2.9%	82.530	0.7%	81.972	1.4%	84.644	1.9%	82.572	0.6%
37	84.8	87.732	3.5%	84.811	0.0%	84.590	0.2%	87.063	2.7%	84.546	0.3%
38	84.4	84.222	0.2%	81.600	3.3%	81.665	3.2%	83.944	0.5%	82.101	2.7%
39	110.71	96.327	13.0%	93.909	15.2%	93.002	16.0%	94.763	14.4%	93.787	15.3%
40	84.30	93.566	11.0%	91.207	8.2%	90.950	7.9%	92.592	9.8%	91.123	8.1%
41	84.89	93.609	10.3%	91.200	7.4%	90.808	7.0%	92.511	9.0%	91.334	7.6%
42	100.50	103.135	2.6%	99.952	0.5%	99.398	1.1%	101.963	1.5%	99.255	1.2%
43	127.20	125.129	1.6%	122.232	3.9%	124.337	2.3%	124.442	2.2%	124.037	2.5%
44	174.09	168.944	3.0%	165.738	4.8%	166.591	4.3%	167.168	4.0%	165.920	4.7%

Appendix C. B97-D Benchmark Data.

Operator		B97-D									
Basis Set		6-31G(d)		6-31+G(d,p)		6-311G++(2d,p)		cc-PVDZ		aug-cc-pVDZ	
Reaction #	Literature B.D.E (Kcal/mol)	Calculated B.D.E (Kcal/mol)	% Error	Calculated B.D.E (Kcal/mol)	% Error	Calculated B.D.E (Kcal/mol)	% Error	Calculated B.D.E (Kcal/mol)	% Error	Calculated B.D.E (Kcal/mol)	% Error
1	105.0	103.622	1.3%	103.381	1.5%	102.014	2.8%	101.932	2.9%	101.153	3.7%
2	100.5	98.584	1.9%	98.350	2.1%	96.715	3.8%	96.456	4.0%	95.905	4.6%
3	99.9	99.115	0.8%	99.097	0.8%	97.489	2.4%	97.461	2.4%	96.773	3.1%
4	98.1	94.701	3.5%	94.619	3.5%	92.879	5.3%	92.482	5.7%	92.217	6.0%
5	100.7	98.981	1.7%	99.019	1.7%	97.469	3.2%	97.363	3.3%	96.715	4.0%
6	98.3	95.173	3.2%	95.118	3.2%	93.325	5.1%	93.026	5.4%	92.696	5.7%
7	100.19	99.093	1.1%	98.906	1.3%	97.185	3.0%	97.285	2.9%	96.600	3.6%
8	99.21	95.147	4.1%	95.094	4.1%	93.309	5.9%	92.987	6.3%	92.685	6.6%
9	98.0	95.124	2.9%	95.064	3.0%	93.287	4.8%	92.977	5.1%	92.700	5.4%
10	98.0	95.115	2.9%	95.060	3.0%	93.288	4.8%	92.969	5.1%	92.686	5.4%
11	111.21	107.192	3.6%	107.574	3.3%	105.851	4.8%	105.158	5.4%	105.151	5.4%
12	111.1	108.329	2.5%	108.559	2.3%	106.874	3.8%	106.344	4.3%	106.173	4.4%
13	88.2	83.529	5.3%	83.763	5.0%	82.317	6.7%	81.772	7.3%	81.509	7.6%
14	98.1	99.362	1.3%	99.241	1.2%	97.679	0.4%	97.235	0.9%	96.882	1.2%
15	81.50	79.194	2.8%	79.750	2.1%	78.215	4.0%	77.421	5.0%	77.579	4.8%
16	85.3	82.606	3.2%	82.653	3.1%	81.168	4.8%	80.657	5.4%	80.388	5.8%
17	82.5	77.974	5.5%	80.334	2.6%	78.819	4.5%	78.159	5.3%	78.255	5.1%
18	76.60	68.204	11.0%	69.183	9.7%	67.834	11.4%	66.758	12.9%	67.122	12.4%
19	82.5	81.290	1.5%	81.609	1.1%	80.024	3.0%	79.377	3.8%	79.334	3.8%
20	83.4	80.468	3.5%	80.243	3.8%	78.745	5.6%	78.048	6.4%	78.180	6.3%
21	83.4	79.634	4.5%	80.153	3.9%	78.658	5.7%	77.987	6.5%	78.115	6.3%
22	81.9	78.932	3.6%	81.789	0.1%	80.242	2.0%	79.589	2.8%	79.558	2.9%
23	95.48	95.825	0.4%	95.776	0.3%	94.202	1.3%	93.484	2.1%	93.588	2.0%
24	95.60	92.932	2.8%	93.305	2.4%	91.516	4.3%	90.817	5.0%	91.041	4.8%
25	90.2	86.207	4.4%	83.019	8.0%	83.277	7.7%	86.433	4.2%	84.489	6.3%
26	88.79	84.606	4.7%	81.555	8.1%	81.607	8.1%	84.651	4.7%	82.927	6.6%
27	87.31	82.531	5.5%	79.538	8.9%	79.221	9.3%	82.092	6.0%	80.653	7.6%
28	87.50	83.611	4.4%	80.570	7.9%	80.211	8.3%	83.285	4.8%	81.752	6.6%
29	86.1	83.189	3.4%	80.311	6.7%	80.016	7.1%	82.789	3.8%	81.440	5.4%
30	100.0	93.124	6.9%	90.453	9.5%	90.043	10.0%	92.233	7.8%	91.170	8.8%
31	101.6	95.823	5.7%	68.007	33.1%	68.220	32.9%	70.911	30.2%	69.282	31.8%
32	99.81	93.107	6.7%	90.161	9.7%	89.809	10.0%	92.192	7.6%	90.974	8.9%
33	87.19	77.803	10.8%	75.492	13.4%	75.159	13.8%	77.036	11.6%	76.205	12.6%
34	75.00	67.466	10.0%	64.879	13.5%	64.676	13.8%	67.100	10.5%	66.030	12.0%
35	73.3	67.350	8.1%	64.735	11.7%	64.492	12.0%	66.718	9.0%	65.803	10.2%
36	83.1	77.456	6.8%	74.382	10.5%	74.388	10.5%	77.255	7.0%	75.111	9.6%
37	84.8	78.600	7.3%	75.650	10.8%	75.350	11.1%	78.184	7.8%	75.938	10.5%
38	84.4	76.404	9.5%	74.090	12.2%	74.018	12.3%	76.851	8.9%	74.954	11.2%
39	110.71	84.811	23.4%	82.728	25.3%	82.334	25.6%	84.064	24.1%	83.169	24.9%
40	84.30	74.702	11.4%	72.828	13.6%	72.764	13.7%	74.126	12.1%	73.294	13.1%
41	84.89	75.078	11.6%	73.116	13.9%	73.133	13.9%	74.654	12.1%	73.657	13.2%
42	100.50	92.916	7.5%	89.298	11.1%	88.607	11.8%	91.378	9.1%	88.483	12.0%
43	127.20	132.348	4.0%	128.838	1.3%	130.594	2.7%	131.455	3.3%	129.844	2.1%
44	174.09	167.781	3.6%	165.409	5.0%	167.247	3.9%	168.099	3.4%	166.647	4.3%

Appendix D. MP2 Benchmark Data.

Operator		MP2									
Basis Set		6-31G(d)		6-31+G(d,p)		6-311G++(2d,p)		cc-PVDZ		aug-cc-pVDZ	
Reaction #	Literature B.D.E (Kcal/mol)	Calculated B.D.E (Kcal/mol)	% Error	Calculated B.D.E (Kcal/mol)	% Error	Calculated B.D.E (Kcal/mol)	% Error	Calculated B.D.E (Kcal/mol)	% Error	Calculated B.D.E (Kcal/mol)	% Error
1	105.0	94.948	9.6%	97.840	6.8%	98.530	6.2%	97.206	7.4%	97.470	7.2%
2	100.5	92.097	8.4%	95.209	5.3%	95.565	4.9%	94.502	6.0%	94.680	5.8%
3	99.9	92.680	7.2%	96.009	3.9%	96.485	3.4%	95.409	4.5%	95.585	4.3%
4	98.1	89.719	8.5%	93.192	5.0%	93.517	4.7%	92.419	5.8%	92.944	5.3%
5	100.7	92.646	8.0%	95.892	4.8%	96.390	4.3%	95.321	5.3%	95.490	5.2%
6	98.3	90.201	8.2%	93.618	4.8%	93.932	4.4%	92.856	5.5%	93.376	5.0%
7	100.19	91.899	8.3%	95.916	4.3%	96.415	3.8%	95.344	4.8%	95.512	4.7%
8	99.21	89.183	10.1%	93.636	5.6%	93.933	5.3%	92.840	6.4%	93.414	5.8%
9	98.0	90.186	8.0%	93.659	4.4%	93.947	4.1%	92.863	5.2%	93.457	4.6%
10	98.0	90.185	8.0%	93.658	4.4%	93.947	4.1%	92.864	5.2%	93.466	4.6%
11	111.21	106.381	4.3%	111.054	0.1%	110.770	0.4%	109.826	1.2%	110.628	0.5%
12	111.1	108.208	2.6%	111.698	0.5%	111.517	0.4%	110.665	0.4%	111.369	0.2%
13	88.2	84.688	4.0%	101.054	14.6%	101.213	14.8%	101.025	14.5%	101.172	14.7%
14	98.1	93.951	4.2%	97.150	1.0%	96.946	1.2%	97.388	0.7%	98.666	0.6%
15	81.50	80.604	1.1%	85.302	4.7%	85.830	5.3%	84.499	3.7%	85.635	5.1%
16	85.3	95.539	12.0%	87.293	2.3%	87.979	3.1%	86.904	1.9%	87.526	2.6%
17	82.5	94.996	15.1%	85.701	3.9%	86.356	4.7%	85.012	3.0%	86.182	4.5%
18	76.60	78.108	2.0%	82.988	8.3%	83.532	9.0%	82.156	7.3%	83.708	9.3%
19	82.5	92.504	12.1%	88.563	7.3%	88.975	7.8%	87.844	6.5%	88.599	7.4%
20	83.4	94.983	13.9%	85.577	2.6%	86.242	3.4%	84.899	1.8%	86.065	3.2%
21	83.4	95.008	13.9%	85.587	2.6%	86.248	3.4%	84.906	1.8%	86.102	3.2%
22	81.9	92.965	13.5%	88.735	8.3%	89.082	8.8%	88.074	7.5%	88.521	8.1%
23	95.48	90.346	5.4%	94.974	0.5%	94.868	0.6%	92.976	2.6%	94.226	1.3%
24	95.60	88.624	7.3%	93.477	2.2%	93.448	2.3%	91.815	4.0%	93.177	2.5%
25	90.2	88.555	1.8%	86.400	4.2%	87.216	3.3%	88.238	2.2%	87.771	2.7%
26	88.79	89.618	0.9%	87.675	1.3%	88.819	0.0%	89.471	0.8%	89.559	0.9%
27	87.31	90.010	3.1%	88.320	1.2%	89.665	2.7%	89.973	3.1%	90.584	3.8%
28	87.50	91.143	4.2%	89.378	2.1%	90.909	3.9%	91.094	4.1%	91.893	5.0%
29	86.1	90.927	5.6%	89.312	3.7%	90.699	5.3%	90.777	5.4%	91.855	6.7%
30	100.0	112.023	12.0%	105.806	5.8%	106.270	6.3%	106.763	6.8%	107.526	7.5%
31	101.6	106.422	4.7%	80.610	20.7%	82.284	19.0%	82.691	18.6%	82.974	18.3%
32	99.81	106.555	6.8%	105.004	5.2%	105.770	6.0%	106.277	6.5%	107.129	7.3%
33	87.19	99.814	14.5%	98.596	13.1%	99.332	13.9%	99.619	14.3%	100.887	15.7%
34	75.00	82.817	10.4%	81.268	8.4%	82.917	10.6%	82.856	10.5%	84.126	12.2%
35	73.3	82.858	13.0%	81.228	10.8%	82.704	12.8%	82.590	12.7%	84.038	14.6%
36	83.1	84.931	2.2%	84.552	1.7%	85.769	3.2%	84.128	1.2%	85.982	3.5%
37	84.8	89.216	5.2%	88.973	4.9%	90.489	6.7%	88.420	4.3%	90.618	6.9%
38	84.4	84.657	0.3%	85.184	0.9%	86.782	2.8%	84.769	0.4%	87.029	3.1%
39	110.71	94.439	14.7%	93.568	15.5%	94.494	14.6%	93.081	15.9%	94.779	14.4%
40	84.30	90.854	7.8%	90.046	6.8%	90.965	7.9%	89.134	5.7%	90.645	7.5%
41	84.89	91.203	7.4%	90.365	6.4%	91.282	7.5%	89.651	5.6%	91.003	7.2%
42	100.50	104.830	4.3%	103.254	2.7%	104.134	3.6%	102.380	1.9%	103.602	3.1%
43	127.20	125.384	1.4%	123.582	2.8%	127.547	0.3%	122.923	3.4%	126.194	0.8%
44	174.09	164.576	5.5%	164.119	5.7%	166.434	4.4%	163.078	6.3%	164.689	5.4%

Appendix E. CBS-QB3 Benchmark Data.

CBS-QB3			
Reaction #	Literature B.D.E (Kcal/mol)	Calculated B.D.E (Kcal/mol)	% Error
1	105.0	103.781	1.2%
2	100.5	99.904	0.6%
3	99.9	100.592	0.7%
4	98.1	97.041	1.1%
5	100.7	100.496	0.2%
6	98.3	97.351	1.0%
7	100.19	100.370	0.2%
8	99.21	97.290	1.9%
9	98.0	97.304	0.7%
10	98.0	97.258	0.8%
11	111.21	109.079	1.9%
12	111.1	109.806	1.2%
13	88.2	85.912	2.6%
14	98.1	100.489	2.4%
15	81.50	82.600	1.3%
16	85.3	84.856	0.5%
17	82.5	83.060	0.7%
18	76.60	72.946	4.8%
19	82.5	84.780	2.8%
20	83.4	82.969	0.5%
21	83.4	82.903	0.6%
22	81.9	85.014	3.8%
23	95.48	98.505	3.2%
24	95.60	96.766	1.2%
25	90.2	88.465	1.9%
26	88.79	88.355	0.5%
27	87.31	87.804	0.6%
28	87.50	88.831	1.5%
29	86.1	88.464	2.7%
30	100.0	98.348	1.7%
31	101.6	75.018	26.2%
32	99.81	97.831	2.0%
33	87.19	84.164	3.5%
34	75.00	73.870	1.5%
35	73.3	73.601	0.4%
36	83.1	83.424	0.4%
37	84.8	86.618	2.1%
38	84.4	83.680	0.9%
39	110.71	93.870	15.2%
40	84.30	87.302	3.6%
41	84.89	87.711	3.3%
42	100.50	100.737	0.2%
43	127.20	127.044	0.1%
44	174.09	173.800	0.2%